Canadian Journal of Research

Issued by THE NATIONAL RESEARCH COUNCIL OF CANADA

VOL. 27, SEC. F. FEBRUARY, 1949 NUMBER 2

DIAMOND DRILL HOLE G-M COUNTER[1]

BY K. FELDMAN[2] AND G. M. WRIGHT[2]

Abstract

A portable instrument for making gamma-ray surveys of diamond drill holes to depths of 1000 ft. is described. The circuit is given in detail.

This instrument was designed for detecting gamma-rays in diamond drill holes of diameter not less than 1.25 in. to depths of 1000 ft. It consists of battery-operated electronic circuits with a G-M tube at the end of a cable, and indicates the counting rate on a rate meter and a loudspeaker. The chassis housing the electronic circuits is fastened to the side of the reel carrying the cable, and rotates with it. The reel is mounted on a portable framework designed to be carried by two men.

Briefly, the circuit works as follows. Each "count" from the G-M tube, attenuated by the cable, is amplified and actuates a trigger circuit. The square pulse thus generated is modulated by a neon oscillator. This modulated pulse, amplified by the power amplifier, gives a note in the loudspeaker and actuates the rate meter.

The Electronic Circuit

The early models of diamond drill hole counter apparatus developed at the National Research Laboratories, Ottawa, consisted of simple circuits similar to those used in other portable counters, with the addition of a probe at the end of a long cable. This probe contained the G-M tube and a suitable amplifier circuit (1). Field experience showed that various modifications were desirable, the most important of which was the elimination of the amplifier circuit in the probe since it frequently gave trouble and was very inconvenient to service.

In the present instrument, these modifications have been made. Only the more unusual features will be described in detail.

(a) G-M Tube and Cable

The G-M tube is of the self-quenching type, requiring an operating voltage of about 1000 v. Both glass and all-metal types have been used, as discussed in a later section on probes.

[1] *Manuscript received November 2, 1948.*

Contribution from the Division of Physics, National Research Laboratories, Ottawa, Canada. Issued as N.R.C. No. 1867.

[2] *Physicist.*

When sufficient amplification is provided at the upper end of the cable, it is found satisfactory to omit the preamplifier in the probe. This not only avoids the trouble previously mentioned but also greatly simplifies the construction and makes it possible to permanently seal the probe. It also eliminates practically all drain on the high voltage circuit, and makes possible the use of a cable having only two conductors of negligible current-carrying capacity.

(b) High Voltage Circuit

The high voltage circuit (V1 and V2, Fig. 1) is of the same type as that previously discussed (1). However, since considerable amplification of the counts is necessary, and since the interconductor capacitance of the cable feeds the ripple from the high voltage circuit directly to the amplifier, it is necessary to add the two-stage filter. It is also necessary to exercise care in wiring, to avoid placing input leads where they might pick up ripple from the high voltage circuit.

(c) Amplifier and Trigger Circuit

The two-stage voltage amplifier (V3 and V4) has a gain of about 2500. The grid resistor in the first stage also serves as the load resistor for the G-M tube. Its value, 15000 ohms, has been chosen to give sufficiently large but not excessively long pulses. With cables having an interconductor capacitance of up to 0.02 μf. this resistance results in pulses up to about one-third of a millisecond in length. For the present application it is considered unnecessary to reduce the pulse length by replacing part of the load resistance with inductance.

The trigger circuit (V5 and V6) is of the conventional type except that the biased tube is a pentagrid converter (V6). Grid No. 3 of this tube serves as the input grid for the neon audio-frequency oscillator (V7). During the conducting periods of V6, i.e., when a pulse trips the trigger circuit, the plate current of this tube is, therefore, modulated at the audio frequency (approximately 1000 c.p.s.). Two sets of coupling constants in the trigger circuit, selected by means of the "OFF-LO-HI" switch, give conducting periods of either 0.25 or 0.001 sec. approximately.

(d) Power Amplifier and Output Circuits

The resistance and capacitance in the coupling between the trigger circuit and the power amplifier (V8) are chosen to differentiate the (negative) pulses from the biased tube. The audio-frequency modulation on each pulse that arrives at the grid of the power amplifier has, therefore, a positive as well as a negative portion. The tube can then be biased to cutoff, thus making it convenient to operate the rate meter in the screen circuit and the speaker in the plate circuit of this tube. As normally used, i.e., with the range switch in the "LO" position, each "count" from the G-M tube thus gives a shrill note about 0.25 secs. long, in the speaker. The pitch of this note is such that it is not easily confused with other sounds in the vicinity, so does not keep the operators under a constant strain. The importance of this is realized when

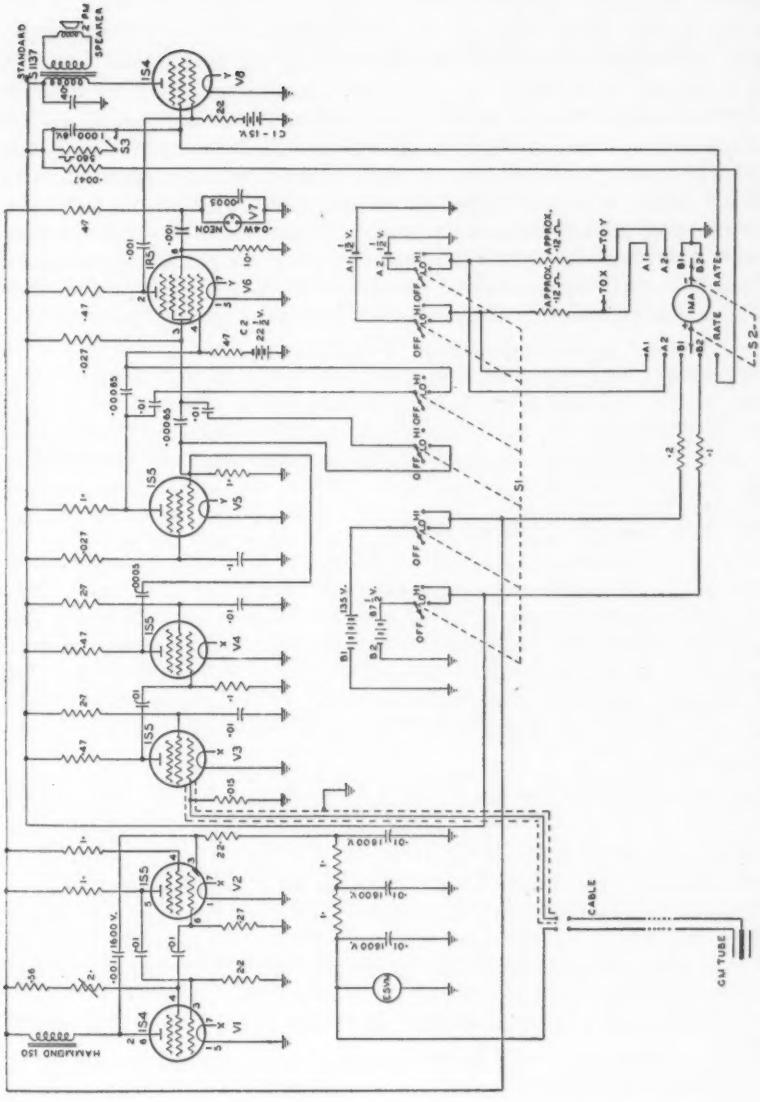

FIG. 1. *Circuit of a portable G-M counter for diamond drill holes. Resistances are given in megohms unless otherwise indicated, capacitances in microfarads.*

it is noted that during a large part of the time only the very low subsurface background activity is encountered. Under such conditions the lowering of the probe is halted to take rate meter readings only at 5 or 10 ft. intervals, yet narrow occurrences in between these points must not be missed.

The rate meter, which measures the averaged screen current in the power amplifier, has a time constant of about five seconds. A pushbutton switch S3 makes it possible to discharge the rate meter capacity quickly when desired. In the "LO" range the rate meter gives a full scale reading for about 200 counts per minute. In the "HI" range (pulse length approximately 0.001 sec.) it has a full scale sensitivity of about 2000 counts per minute. The modulated pulses from the trigger circuit are then too short for the audio tone in the speaker to be recognized as such. However, the higher counting rates that necessitate the use of this range partially compensate for this, and a satisfactory aural signal results. Also, under such conditions the more frequent rate meter readings taken render the aural signal less important.

The rate meter is essentially linear in each range. A decrease of 5 v. in the "B" voltage, however, results in a decrease in sensitivity of about 15%. For the present application this was not considered of sufficient importance to warrant the inclusion of means for setting the "B" voltage at a fixed value. Other factors influencing the sensitivity of the rate meter are discussed in Section (*f*).

(e) Switching, Metering, Batteries, etc.

Two 1.5 v. "A" batteries (such as Eveready No. 742) have adequate capacity to permit continuous operation for several hours at a time. Two separate "B" supplies (made up of 67.5 v. batteries such as Eveready No. 467) are used to eliminate coupling between the input amplifier and the high voltage or neon oscillator circuits. One of these, B1, supplies 135 v. to permit the satisfactory operation of the neon oscillator. The bias supplies, C1 and C2, are provided by miniature batteries such as Eveready No. 411 (15 v.) and No. 412 (22.5 v.).

The switch *S*2 allows the use of the 0–1 ma. meter, normally in the rate meter circuit, for checking the "A" and "B" batteries. It has been found very useful to include, also, an electrostatic voltmeter to constantly indicate the high voltage. The similarity between the low counting rates frequently encountered and the results in more active regions when the operating voltage is slightly too low is otherwise a constant source of worry. Also, problems connected with diagnosing trouble while the probe is hundreds of feet down a hole, or with setting the high voltage under operating conditions where the temperature in a hole is widely different from that at the surface, are greatly simplified.

(f) Selection of Components

Figures quoted above for the rate meter sensitivity, etc., are merely typical values. As may be expected, they vary considerably from unit to unit when commercial components with normal tolerances are used. Also variations in

characteristics of the individual electronic tubes have marked effects. The most important of these are discussed below:

(i) The use of a 135 v. "B" supply instead of the usual 67.5 v. (1) makes the selection of tubes for the high voltage circuit somewhat less critical than would otherwise be the case. However, the statements made in the above reference regarding the suitability of tubes for high voltage circuits still apply to a large extent.

(ii) It has been found that some 1R5 (V6) tubes used in the trigger circuit are not completely cut off by the 22.5 v. bias. In such cases a current of some 20 to 25 μa. flows through the tube. This does not seriously affect the operation of the trigger circuit. However, it does permit a signal from the neon circuit to be continuously passed. This causes a hum in the speaker and a spurious reading on the rate meter. If such tubes are excluded, variations in sensitivity of the rate meter with different 1R5's are slight. Somewhat greater variations in sensitivity, up to $\pm$ 10% are found with different 1S5's (V5).

(iii) The 1S4 in the power amplifier (V8) is sometimes not completely cut off by the 15 v. bias. This again gives rise to a spurious rate meter current, though in this case there is no associated speaker hum. Excessive bias on the other hand would cut down the sensitivity of the rate meter and the volume of the loudspeaker. In practice this spurious rate meter current seldom exceeds 0.05 ma. on the 1 ma. meter, but when such tubes are used the sensitivity of the rate meter may increase by as much as 20%.

Probes

The chief problem in constructing the probe is to make it waterproof under a 1000 ft. head of water. In the case of the glass walled G-M tubes, the tube is placed in a brass cylinder of $1\frac{1}{8}$ in. external diameter. It was found unsatisfactory to use gland type seals at the point where the cable entered the brass cylinder, since under the necessary pressure the cable was deformed by the compressive gland. Probes filled with ceresin wax or with oil were found satisfactory, but are difficult to assemble under field conditions when replacement of the G-M tube becomes necessary.

All-metal, single ended G-M tubes coated with rubber promise to be more satisfactory. In making these probes a short length of cable is connected to the G-M tube. Rubber is then coated over the entire tube, connector, and a portion of the cable, to a diameter of 1 in. The end of the length of cable can be spliced to the main cable in the field without much difficulty.

Reference

1. HUSHLEY, W. and FELDMAN, K. Can. J. Research, F, 25 : 226. 1947.

CANADIAN ERUCIC ACID OILS[1]

III. SHORTENINGS FROM RAPE AND MUSTARD SEED OILS

By H. J. Lips,[2] N. H. Grace,[2] and Suzanne Jegard[3]

Abstract

Processed rape and mustard seed oils were hydrogenated at 50 lb. pressure and 284° F., using a commercial nickel formate catalyst, and were deodorized for one hour at 464° F. The stability of the hardened oils compared favorably with that of a standard commercial vegetable shortening. Taste panel tests indicated that both the rape and mustard shortenings were as satisfactory as the commercial reference material for the preparation of pastry and doughnuts. Special study of the rape product showed that it could be plasticized, and it gave good results in baking volume experiments.

Introduction

In the nonselective hydrogenation of vegetable oils commonly employed in the manufacture of shortening, some (combined) stearic acid is formed by complete saturation of oleic acid, and some elaidic acid by geometrical transformation of oleic acid (2, p. 565). The comparable reactions in erucic acid oils would lead to the formation of behenic and brassidic acids from erucic acid. In view of the widely different melting points and structures of the possible fatty acid products, it might be expected that shortenings from erucic acid oils could differ markedly from those in ordinary use. Moreover, Canadian shortening manufacturers have suggested verbally that hardened erucic acid oils may be inferior in baking volume properties. On the other hand, Canadian rape and mustard seed oils were shown to possess potential value as salad and cooking materials (6), and hardened rape seed oil was eaten during the war in Germany (4), so it might be expected that shortenings from rape and mustard seed oils would be acceptable food products. Estimation of possible consumer reaction to shortenings prepared from these oils by a standard method was therefore undertaken, with special consideration to the effect of rape shortening (the more important product) upon baking volume.

Materials and Methods

The processing of the crude rape and mustard seed oils used in this work has been described (3, 6). In brief, they were refined with 10° Bé. alkali and bleached under nitrogen with 2% Superfiltrol for 20 min. at 212° F.

The oils were then hydrogenated in a pilot-scale, stainless steel hydrogenator of 10 lb. capacity, at 50 lb. pressure and 284° F., with purging at 15 min. intervals. The catalyst was commercial nickel formate (25% nickel) at

[1] *Manuscript received October 4, 1948.*

Contribution from the Division of Applied Biology, National Research Laboratories, Ottawa, Canada. Issued as Paper No. 219 of the Canadian Committee on Food Preservation, and as N.R.C. No. 1875.

[2] *Biochemist, Oils and Fats Laboratory.*

[3] *Biochemist, Food Investigations.*

1% concentration. The course of hardening was followed by withdrawing samples and determining the refractive index. When the desired hardness was reached, the material was removed from the hydrogenator, 1% diatomaceous earth was added, and the mixture was filtered in a porcelain Büchner funnel. The shortening was then steam deodorized under vacuum in an all-glass apparatus for one hour at 464° F. Each test shortening was a composite of two or three individual preparations. A standard commercial vegetable shortening of high quality was used as reference material in all tests, and comparisons were made both with fresh shortenings and shortenings aged for 10 days at 100° F.

Color, fluorescence, kinematic viscosity, peroxide oxygen, free fatty acid, and smoke point were measured at different stages of use of these materials, as previously described (3, 6). Iodine value was determined by a modification of Wij's method (5) and melting point by the capillary tube method (1).

Pastry and doughnuts were prepared with the shortenings according to the recipes given in Table I. Pastry was baked 10 min. at 435° F. and served at

TABLE I

RECIPES FOR DOUGHNUTS AND PASTRY, GIVEN IN GRAMS

Constituent	Doughnuts	Pastry
Eggs	96	—
Flour	500	112
Sugar	200	—
Shortening	25	66
Milk	224	—
Water	—	30
Baking powder	15	—
Cinnamon	½	—
Nutmeg	½	—
Salt	4	2

room temperature; doughnuts were fried in the shortenings at 355° to 365° F. for three minutes and served warm. Pastry and doughnuts were scored for taste and odor by a 24-member panel as previously described (6); excess or deficiency of the property was rated on an integral scale of + 5 to − 5.

After some preliminary trials, the following biscuit volume method (Method *A*) was developed to determine the effect of shortenings on baking volume: 100 gm. of flour, 3.5 gm. of baking powder, and 1.3 gm. of salt were mixed for one minute in a jacketed dough mixer held at 100° F. Fat (17 gm.) warmed to a temperature of 140° F. was added to the dry mixture and the mixing process continued for another minute, then 50 ml. of water was added and mixed in for one minute more. The total mixing time was three minutes. A 100 gm. sample of this batter was weighed into a small baking tin and baked for 30 min. at 475° F. The volume of the baked biscuit was measured

by a rapeseed displacement method (7). In variations of this procedure, 60 ml. of water was used instead of 50 ml. (Method *B*); and unmelted rather than melted fat was used (Method *C*).

Results

Shortening Measurements

Tables II and III present physical and chemical measurements for the commercial, mustard, and rape shortenings. The commercial shortening had a lower iodine value and melting point (Table II) than the rape and mustard

TABLE II

CHARACTERISTICS OF SHORTENINGS USED FOR TASTE PANEL TESTS

Shortening	Melting point, ° C.	Iodine value
Commercial	38.0	57.9
Mustard	42.9	67.6
Rape	45.4	58.3

shortenings of about the same hardness chosen for comparative test. The relative transmissions at 440 and 660 mμ of the rape and mustard products were similar, and slightly less than those of the commercial material (Table III). Indications were (Table III, *C*) that the color was not sufficiently intense to interfere with the measurement of fluorescence. Fluorescence in ultraviolet light (375 mμ) increased in the order: rape, commercial, mustard; and viscosity in the order: commercial, mustard, rape. Peroxide and free fatty acid values were uniformly low. The commercial shortening had the highest smoke point, with rape shortening next, and mustard shortening lowest but still fairly satisfactory.

These characteristics were altered in varying degree by aging the shortenings or by using them for the deep fat frying of doughnuts (Table III): transmission was not changed by aging but decreased markedly with frying; fluorescence increased with frying; viscosity was practically constant;

TABLE III

CHEMICAL AND PHYSICAL MEASUREMENTS ON SHORTENINGS AT VARIOUS STAGES OF USE

Shortening	Condition of shortening			
	Fresh	Aged	Fresh, fried	Aged, fried
	Measurement			
	A. Transmission, per cent at 440 mμ and 60° C., relative to mineral oil (Stanolax)			
Commercial	68	68	48	56
Mustard	58	55	38	36
Rape	61	61	48	35

TABLE III—*Concluded*

CHEMICAL AND PHYSICAL MEASUREMENTS ON SHORTENINGS AT VARIOUS STAGES OF USE—*Concluded*

Shortening	Condition of shortening			
	Fresh	Aged	Fresh, fried	Aged, fried
	Measurement			
	B. As in A, at 660 mμ			
Commercial	98	97	95	97
Mustard	92	92	96	96
Rape	90	91	95	94
	C. Transmission, per cent at 440 mμ of 1 gm. of shortening in 100 ml. xylol, relative to xylol			
Commercial	99	100	99	100
Mustard	99	99	99	99
Rape	100	99	99	98
	D. Fluorescence, Coleman photofluorometer units, 1 gm. of oil in 100 ml. xylol, corrected for fluorescence of xylol			
Commercial	16	13	18	18
Mustard	32	33	38	38
Rape	12	10	19	17
	E. Viscosity, centistokes at 130° F.			
Commercial	27.2	27.6	27.2	27.5
Mustard	30.6	30.4	30.2	30.2
Rape	33.3	33.8	34.0	33.8
	F. Peroxide value, ml. of 0.002 N thiosulphate per gm.			
Commercial	0.0	0.0	2.8	4.9
Mustard	0.0	0.0	4.3	3.9
Rape	0.0	0.0	3.8	3.7
	G. Free fatty acid content, as % oleic acid			
Commercial	—	—	0.1	0.1
Mustard	—	—	0.2	0.2
Rape	—	—	0.2	0.2
	H. Smoke point, ° F.			
Commercial	430	427	398	399
Mustard	387	385	385	372
Rape	414	410	388	382

peroxides were detectable only in the fried shortenings; smoke points were lowered slightly by aging, and to a greater extent by frying.

Taste Panel Tests

Taste panel ratings for all pastry and doughnut products (Table IV) showed no difference between doughnuts prepared from any of the types of shortening tested but, on the average, odor and flavor of pastry made with the experimental fats were rated as slightly preferable to those of pastry made with similar amounts of the commercial shortening.

TABLE IV

AVERAGE PANEL SCORES FOR ODOR AND FLAVOR OF PASTRY AND DOUGHNUTS

Shortenings	Pastry		Doughnuts	
	Odor	Flavor	Odor	Flavor
Fresh:				
Commercial	+ 0.5	+ 0.4	+ 0.1	+ 0.1
Mustard	+ 0.1	+ 0.1	+ 0.2	+ 0.1
Rape	+ 0.2	+ 0.2	+ 0.1	+ 0.2
Aged:				
Commercial	+ 0.5	+ 0.7	+ 0.2	+ 0.2
Mustard	+ 0.1	+ 0.2	+ 0.2	+ 0.2
Rape	+ 0.1	+ 0.2	+ 0.2	+ 0.2
Necessary difference (5% level of statistical significance)	± 0.4	± 0.4	± 0.3	± 0.4

Baking Volume

Different samples of hydrogenated rapeseed oil, with iodine values from 40 to 100, showed no significant volume difference by baking methods *A* or *B* in two series of hydrogenated oils (Table V). The additional water added in Method *B* caused a general increase in baking volume that was significant for most of the shortenings tested. However, when unmelted fat was used (Method *C*), the rapeseed biscuits were significantly smaller than the reference biscuits if the hydrogenated oil had an iodine number less than about 85. Biscuits made from the commercial product had the same baking volume regardless of the state of the fat. These results indicated that when the unmelted rapeseed shortening was used some physical factor interfered with fat distribution in the mixture and resulted in an inferior baking volume.

The hydrogenated rapeseed oil was then plasticized to make its consistency approximate more closely that of the standard commercial shortening. The steps in the plasticizing process were: (*a*) preliminary heating of the fat to 212° F., (*b*) beating of the melted fat in a Mixmaster with rapid cooling at −40° F. until the mass solidified, and (*c*) tempering the plasticized product at 80° F. for three days. Two samples of plasticized fat were prepared from

TABLE V

COMPARATIVE BISCUIT VOLUMES FOR HYDROGENATED RAPESEED OILS AND A COMMERCIAL VEGETABLE SHORTENING

(Averages of three determinations)

Description of samples			Biscuit volume, ml.		
Shortening	Iodine No.	M.p., °C.	Method *A* (50 ml. water)	Method *B* (60 ml. water)	Method *C* (unmelted fat)
Standard (commercial vegetable shortening)	57.9	38.0	195	210	195
Hardened rapeseed oils, samples taken at intervals during hydrogenation:					
Hydrogenation series I	103.2	< 15.0	204	208	—
	90.0	18.0	199	212	—
	65.9	42.0	200	214	—
	49.2	49.8	196	—	—
	44.5	52.0	199	210	—
Hydrogenation series II	100.5	< 15.0	198	—	194
	87.8	23.3	202	—	186
	63.8	42.8	197	—	183
	55.0	47.6	197	—	184
Necessary difference (5% level of statistical significance)			10		

a rapeseed shortening of melting point 46° C., which was higher than the melting point of the commercial shortening (38° C.). The plasticized products were found to have good mixing properties in the solid form. Biscuits were baked with the fat in an unmelted state. The resulting volumes were:

Unplasticized — 184 ml.

Plasticized sample No. 1 — 191 ml.

Plasticized sample No. 2 — 196 ml. (a significantly higher figure than for the same material unplasticized)

Commercial — 195 ml.

These figures showed that the hydrogenated rapeseed oil could be plasticized to give as good a biscuit volume as the standard commercial vegetable shortening.

Conclusions

Hardened erucic acid oils prepared by a standard method did not differ markedly from ordinary shortening in the properties studied, in spite of inherent compositional differences. No special hardening techniques were necessary to prepare shortenings acceptable as food products from processed

Canadian rape and mustard seed oils. These shortenings were stable materials of fair color and smoke point, and were amenable to plasticization and use in baking.

Acknowledgments

The statistical aid of Dr. J. W. Hopkins, the technical supervision of odor and flavor appraisals by Miss E. M. Hamilton, and the technical assistance of Miss K. Stewart and Mr. A. C. Bell are all gratefully acknowledged.

References

1. AMERICAN OIL CHEMISTS' SOCIETY. Official and tentative methods. 2nd ed. A.O.C.S., Chicago. 1946.
2. BAILEY, A. E. Industrial oil and fat products. Interscience Publishers, Inc., New York. 1945.
3. GRACE, N. H. Can. J. Research, F, 26 : 349-359. 1948.
4. GRACE, N. H. and ZUCKERMAN, A. Can. Chem. Process Inds. 31 : 571-572. 1947.
5. HUNTER, L. and HYDE, F. F. Analyst, 58 : 523-527. 1933.
6. LIPS, H. J., GRACE, N. H., and HAMILTON, E. M. Can. J. Research, F, 26 : 360-365. 1948.
7. MALLOCH, J. G. and COOK, W. H. Cereal Chem. 7 : 307-310. 1930.

LABORATORY STUDY OF LOW RATIO BUTADIENE–STYRENE COPOLYMERS[1]

By J. M. Mitchell[2] and H. Leverne Williams[3]

Abstract

The copolymerization of styrene and butadiene in ratios in which the styrene equals or predominates over the butadiene on a mass basis is essentially similar to copolymerization in the presence of a predominance of butadiene. However, the rate of reaction and the length of the induction period is increased. Increasing the amount of the dodecyl mercaptan regulator results in a slight increase in rate and diminution of the induction period. The dodecyl mercaptan reacts at a lower rate than during the production of GR–S. The regulating index as defined by the ratio of the logarithm of the residual mercaptan over the conversion is 1.53. The bound styrene and increment styrene curves seem to be normal and indicate reactivity ratios r_1 (butadiene) equal to 1.4 to 2.2, r_2 equal to 0.5 to 0.7. If these reactivity ratios are corrected for the bifunctional nature of butadiene then the constants for butadiene monomer are Q equal to 0.9 and e equal to -1. Likewise the gel–viscosity data are similar to those observed with GR–S except that the pre-gel rise in viscosity, the formation of gel, and the slope of the viscosity conversion curves diminish with increasing styrene in the charge. The chain transfer action of styrene is increasingly evident with increasing styrene content in the charge but in all cases the regulating effect of dodecyl mercaptan is still apparent.

Introduction

Butadiene and styrene may be copolymerized in all proportions and the resulting copolymers vary in their characteristics between the properties of pure polybutadiene and pure polystyrene but not necessarily like a mechanical mixture of the two pure polymers in the same proportions. An earlier investigation (20, 21) described the effect of the change of butadiene-to-styrene ratio from 90/10 to 50/50 on the physical properties of rubber vulcanizates. Preliminary to a similar study in the lower butadiene to styrene ratios, it was essential to obtain certain small scale laboratory data similar to those described in numerous publications for chemical rubber. Only scattered data of this type are available. Meehan (23) has studied the composition of copolymers over both ranges. Fragmentary data are in the various papers on the use of the copolymers (1, 5, 6, 7, 9, 11, 15, 19, 26, 27, 31, 32) as fillers, reinforcers, resins, or rubbers.

Techniques

All reactions were conducted in 8-oz. screw cap bottles fitted with a gasket (12) for syringe sampling (14). The soap solutions, styrene, and regulator and, for the 15/85 ratio copolymers, the initiator were weighed into the bottle and a slight excess of butadiene added. The excess butadiene was allowed to vaporize to drive out the air in the bottle, which was capped when it had reached the correct weight. The bottles were then placed in the constant

[1] *Manuscript received September 3, 1948.*

Contribution from the Physical Chemistry Research Laboratory, Research and Development Division, Polymer Corporation Limited, Sarnia, Ont.

[2] *Junior Chemist.*

[3] *Research Chemist.*

temperature bath and rotated end over end for 30 min. until they had reached the desired temperature. At that time, usually, the initiator solution was injected by syringe and needle and the agitation resumed. The initiator was added before capping the 15/85 charges since these soon developed, inside, a low pressure which tended to suck water through the punctured self-sealing gasket. Nitrogen pressure was used to facilitate sampling at the end of the reaction. After the appropriate time a sample was removed by syringe and needle and a known weight of latex dried to determine the conversion of hydrocarbon to resin. Just before the reaction was stopped, a 10 ml. syringe sample of the latex was obtained, on which a duplicate determination of unreacted mercaptan was done by amperometric titration (16) with 0.005 *N* silver nitrate.

When the reaction was to be terminated, the solution of hydroquinone was injected into the bottle, which was then shaken vigorously and allowed to cool. After the reaction was stopped, the final conversion of hydrocarbon to resin was determined on each sample using the unvented solids technique. Excess butadiene was vented by insertion of a needle through the gasket and finally excess monomers were removed by steam distillation.

Recovery of the polymer was effected by coagulating one-half of the latex with sodium chloride – sulphuric acid mixture, washing the coagulum, and drying. If the polymer were to be preserved then sufficient BLE dispersion was added before coagulation to give 1.5% BLE based upon the dry resin.

Dilute solution viscosities were measured as reported earlier (8), i.e., by the four-point method using a modified Ubbelohde pipette and benzene as solvent. Corrections for nonrubber solids in the dry polymer are shown in Table I and are applicable to all polymers prepared in the recipe shown in

TABLE I

PER CENT RESIN IN DRY PRODUCT AT VARIOUS CONVERSIONS

Conversion, %	Total solids based on 100 parts monomer charge, %	Resin in dry product corrected for 1.5 parts BLE, %
0	6.11	0
1	7.11	13.9
2	8.11	24.3
3	9.11	32.4
5	11.11	44.4
10	16.11	61.2
15	21.11	70.0
20	26.11	75.5
30	36.11	81.9
40	46.11	85.5
50	56.11	87.8
60	66.11	89.5
80	86.11	91.5
100	106.11	92.9

Table III regardless of the charge ratio. The amount of gel (benzene insoluble) was the difference between the mass of polymer placed in benzene and the amount that dissolved. The swelling index was the ratio of the weight of swollen gel and imbibed solvent to the weight of dry gel.

The remaining unstabilized latex was coagulated with isopropanol and given three successive, five minute washes in fresh alcohol to remove all alcohol soluble materials. The polymer was dried at 100° C. in a vacuum oven for three hours, sheeted on a tight mill, and its refractive index measured at 60° C., using an Abbé refractometer through which water at 60° C. was circulated. The bound styrene of those polymers prepared with 70 to 85 parts of styrene in the charge was read from a graph relating it to the refractive index at 60° C. A straight line relation between GR-S chemical rubber and polystyrene was assumed; and a check on the values was obtained by using a soft polymer and the familiar refractive index technique at 25° C. involving the equation

$$\text{Bound styrene} = 22.94 + 1180\,(n_D^{25} - 1.5339) - 2340\,(n_D^{25} - 1.5339)^2.$$

The cross check data are shown in Table II and indicate that the answers agree very well. The results measured at 60° C. may be 1 to 2% higher than those measured at 25° C. The bound styrene of the 50/50 ratio copolymers was measured at 25° C.

TABLE II

CROSSCHECK DATA ON REFRACTIVE INDICES

Sample No.	n_D^{60}	Styrene in resin, %	n_D^{25}	Styrene in resin, %
1	1.5527	58.0	1.5650	57.4
2	1.5531	58.4	1.5654	57.7
3	1.5559	61.9	1.5690	61.4
4	1.5586	64.6	1.5712	63.7
5	1.5616	68.4	1.5743	66.8

Experimental

The basic charge formula resembled those in general use and is shown in Table III. It was very similar to that used in the preparation of Rubber Reserve polymer X-323. At 50° C. as used for GR–S chemical rubber the reaction was too rapid, especially when the 20/80 and 10/90 butadiene–styrene ratios were used. To obtain adequate results the samples were prepared at 45° C. A preliminary survey of the field yielded the data in Table IV. In all cases 0.15 part of dodecyl mercaptan was used, based upon the monomers.

These data indicated that no serious difficulty was to be expected and it was decided to investigate three monomer ratios in greater detail. The effect of charge ratio of butadiene to styrene and amount of dodecyl mercaptan charged upon rate is shown in Fig. 1. It is evident that as the amount of

TABLE III

FORMULA FOR POLYMERIZATION SYSTEM

Butadiene (commercial pure)	Variable	Total 50 gm.
Styrene (commercial pure)	Variable	
Dodecyl mercaptan	Variable	
S.F. soap flakes, gm.	2.25	
Daxad 11,* gm.	0.50	
Potassium persulphate, gm.	0.15	(6 ml. of 2.50% sol'n.)
Distilled water, gm.	112.50	
Stopping agent hydroquinone, gm.	0.08	(2 ml. of 4% sol'n.)
Antioxidant BLE*, %	1.5	Based upon dry resin

* *Trade names, no simple chemical formula.*

TABLE IV

COPOLYMERIZATION OF STYRENE AND BUTADIENE IN VARIOUS RATIOS

Butadiene to styrene charge ratio, parts	Reaction time, hr.	Conv. %	Gel, %	Swelling index	$[\eta]$
50/50	$4\frac{1}{4}$	18.5	1	—	2.06
"	8	55.5	9	36	2.42
"	12	64.2	65	60	2.44
"	16	78.8	74	70	1.05
40/60	$4\frac{1}{4}$	21.5	10	52	2.45
"	8	58.5	4	26	3.04
"	12	71.3	71	82	1.58
"	16	—	—	—	—
30/70	4	21.6	4	—	1.25
"	8	55.3	6	—	1.36
"	$13\frac{2}{3}$	85.3	73	53	2.28
20/80	$2\frac{1}{2}$	9.1	—	—	—
"	$5\frac{1}{6}$	38.6	—	—	—
"	$7\frac{1}{2}$	58.5	—	—	—
"	12	89.5	—	—	—
10/90	$2\frac{1}{2}$	6.9	—	—	—
"	$5\frac{1}{6}$	34.0	—	—	—
"	$7\frac{1}{2}$	73.7	—	—	—
"	12	93.5	—	—	—

butadiene in the charge is diminished there was an increase in the rate of conversion to resin. At 45° C. the rate was about twice as great with 15/85 ratio as with the 50/50. Also it can be seen, particularly in the case of the 50/50 ratio that the increasing amount of mercaptan resulted in a greater yield in a given time by shortening the initial induction period. It is evident, too, that increasing the styrene in the charge had lengthened the induction period slightly. This could be due to either the increased difficulty of purging the bottles of air or to the increased inhibitor added with the styrene. The conversion of monomers to GR–S at 50° C. would be very similar to the lower broken curve of Fig. 1.

The rate of disappearance of dodecyl mercaptan was insensitive to charge ratio of butadiene to styrene and to the amount of mercaptan charged within

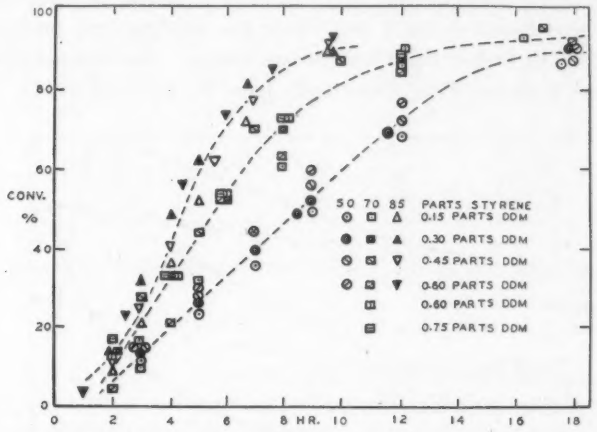

FIG. 1. *Time–conversion curves for various ratios of butadiene to styrene and with various amounts of dodecyl mercaptan at 45° C. Broken lines represent average curve. Time–conversion curve for GR–S at 50° C. is almost identical with the lower broken curve.*

the limits studied, as shown in Fig. 2. The data when an average curve was estimated indicated slight or negligible consumption of mercaptan during the first few per cent conversion of hydrocarbon to resin when 70, and particularly 85, parts of styrene were charged. A representative curve for GR–S is shown and can be seen to lie below all the experimental data of this series.

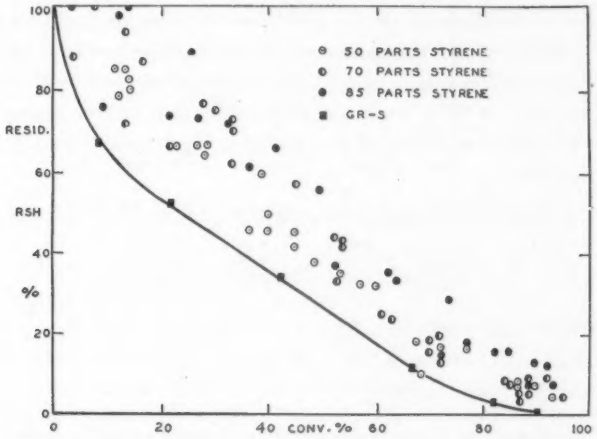

FIG. 2. *Residual mercaptan for various charge ratios of butadiene to styrene and all amounts of dodecyl mercaptan charged as a function of conversion at 45° C. Lower curve is a typical result for GR–S at 50° C.*

If the data were plotted in the form *ln* (% residual mercaptan) versus per cent conversion the initial slope of the straight line portion became by definition the regulating index. For all three charge ratios and all mercaptan charges this was found to be 1.53. Since the straight line portion extrapolates to 100% or higher there is no waste factor. The comparable figures for GR–S were 2.39 and 19% respectively from the curve of Fig. 2.

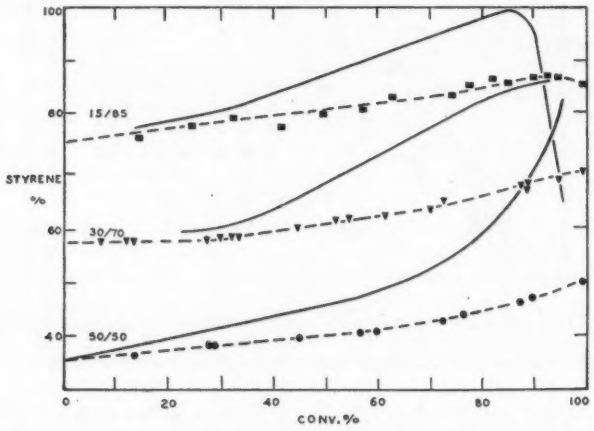

FIG. 3. *Bound styrene (broken lines) and increment styrene (solid lines) for various charge ratios of butadiene to styrene as a function of conversion at 45° C.*

The bound styrene, Fig. 3, followed the same general form (20, 21, 23) as those published previously. The data for the 30/70 butadiene-to-styrene ratio indicated a leveling off of the increment styrene at higher conversions. This was accentuated and the increment styrene curve reversed for the 15/85 ratio. The explanation might be that the refractometric method of measuring the bound styrene at 60° C. was, indeed, indicating values about 2% high. A more precise measure of bound styrene over this range would be necessary to clarify the cause.

From the general copolymerization equation (2, 3, 22, 28)

$$\frac{d[M_1]}{d[M_2]} = \frac{[M_1]}{[M_2]} \times \frac{r_1[M_1] + [M_2]}{r_2[M_2] + [M_1]}$$

and assuming an ideal case, i.e.,

$$\frac{d[M_1]}{d[M_2]} = \alpha \frac{[M_1]}{[M_2]} = \alpha R,$$

the values of R and α have been calculated for the three ratios from the bound styrene data obtained by extrapolating to zero conversion. The data are in Table V.

TABLE V

REACTIVITY RATIO CALCULATIONS

Butadiene-to-styrene charge ratio	$d[M_2]$ Styrene at 0 conv., %	$d[M_1]$ Butadiene at 0 conv., %	$\frac{d[M_1]}{d[M_2]}$	R	α
50/50	34.8	65.2	1.872	1.00	1.87
30/70	57.8	42.2	0.729	0.429	1.70
15/85	75.6	24.4	0.323	0.177	1.82

Using the values of R and α the values of r_1 and r_2 were calculated from the equation

$$r_1 = \frac{\alpha}{R} r_2 + \left(\alpha - \frac{1}{R}\right),$$

and plotted as in Fig. 4. From the dimensions of the resultant triangle the value of r_1, the ratio of the reactivity of butadiene radical with butadiene over its reactivity with styrene, ranged from 1.4 to 2.2, whereas r_2, the ratio of the reactivity of the styrene radical with styrene over the reactivity with butadiene, lay between 0.5 and 0.7.

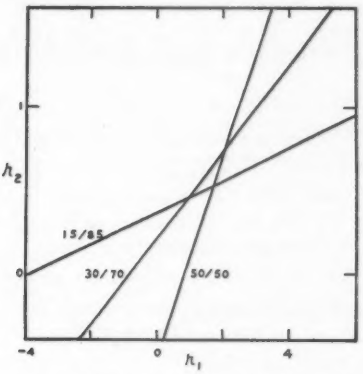

FIG. 4. *Plot of r_1 versus r_2 to obtain the range of the probable values of the reactivity ratios.*

These reactivity ratios were calculated on a molar basis without regard for the two double bonds present in butadiene. Assuming that each of these double bonds possessed the same reactivity, the reactivity ratios may be corrected for the two double bonds, that is, converted to a "double bond" rather than molar basis. When this is done the characteristic constants Q and e (4) may be calculated (4, 10). These were 0.9 and -1 for butadiene. Q may be considered the mean reactivity of the butadiene double bond and e may be considered proportional to the charge on the butadiene radical and group relative to Q and e for styrene of 1 and -1 respectively.

The gel and viscosity data for the 50/50 ratio copolymers are shown in Fig. 5. It was apparent that, as polymerization proceeded, the dilute solution viscosity of the polymer rose slowly. Then at fairly high conversions cross

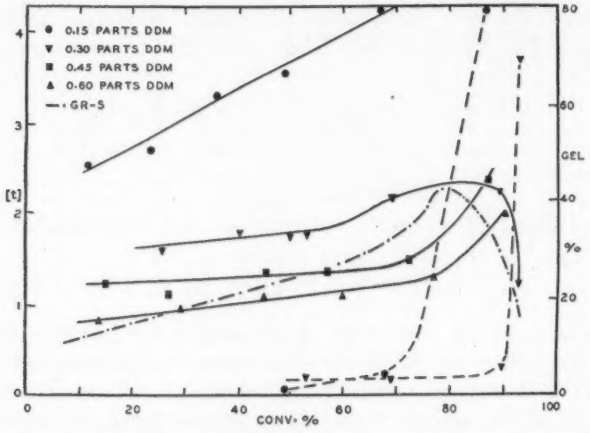

FIG. 5. *Dilute solution viscosity (solid line) and gel (broken line) data for 50/50 butadiene to styrene copolymers with various amounts of dodecyl mercaptan in the charge as a function of conversion at 45° C. Curve (—·) is a typical one for GR-S at 50° C.*

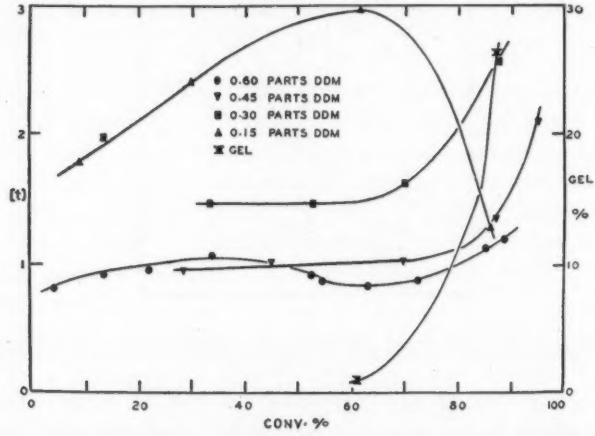

FIG. 6. *Dilute solution viscosity and gel (0.15 parts DDM only) data for 30/70 butadiene-to-styrene copolymers with various amounts of dodecyl mercaptan in the charge as a function of conversion at 45° C.*

linking and branching started, at which time the viscosity rose rapidly, then fell sharply when gel formed and was removed, leaving only low molecular weight material. It is evident also that, as the amount of dodecyl mercaptan regulator added was increased, the viscosity, i.e., molecular weight, of the

copolymer was diminished and the rise in the viscosity with conversion was less marked and more delayed. These same observations were noted with the 30/70 ratio copolymers, Fig. 6. In this case the polymers prepared using 0.60 part of dodecyl mercaptan seemed to be out of line. However, no irregularity was noted with the 15/85 ratio, Fig. 7. In this the viscosity of the

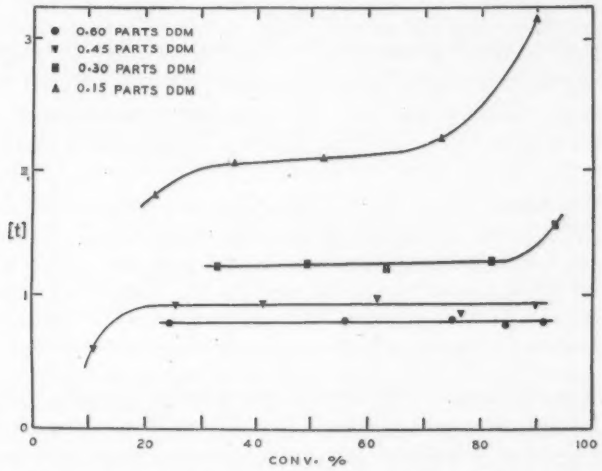

FIG. 7. *Dilute solution viscosity data for 15/85 butadiene-to-styrene copolymers with various amounts of dodecyl mercaptan in the charge as a function of conversion at 45° C.*

polymer remained remarkably constant up to quite high conversions before there was the increase in viscosity with conversion. Comparison of Figs. 5, 6, and 7 will show that under comparable conditions the increase in styrene in the charge resulted in a lower viscosity polymer by increased chain transfer due to the styrene, and the formation of higher molecular weight material including gel is delayed. Additional data over a narrow range of concentrations and pertaining to the 30/70 ratio in the proximity of the normal commercial conversion range are in Table VI. The reaction time was 10.5 hr. at 45° C.

TABLE VI

MERCAPTAN–VISCOSITY RELATION

Resin	Conversion, %	Gel, %	[t]	Parts dodecyl mercaptan
1	77.7	4	1.30	0.45
2	78.2	1	1.43	0.35
3	77.9	3	1.47	0.30
4	78.0	1	1.98	0.25
5	77.0	6	2.83	0.15

The effect of the butadiene-to-styrene ratio in the charge is likewise amply demonstrated by the data in Table VII, which shows a comparison of three copolymers of general commercial use. With increasing styrene in the charge the rate of the reaction was increased and the amount of dodecyl mercaptan required for approximately the same dilute solution viscosity and solubility was reduced.

TABLE VII

DODECYL MERCAPTAN REQUIREMENTS FOR COPOLYMERS OF COMPARABLE VISCOSITY

	Butadiene to styrene ratio		
	70/30	50/50	30/70
Parts dodecyl mercaptan	0.425	0.320	0.214
Reaction time, hr.	13	$8\frac{2}{3}$	$5\frac{1}{3}$
Solids, %	27.4	23.8	23.0
Conversion, %	74.3	74.0	70.3
Soluble in benzene, %	96	95	89
Gel, %	4	5	11
$[t]$	1.92	2.16	2.20

Although in all cases the corrected dilute solution viscosity was measured using dry polymer, it was of interest to try the modified vistex viscosity technique whereby latex is dissolved in mixed solvents, benzene/isopropanol 80/20, and diluted by successive portions of benzene in the usual manner. Plotting the data allows extrapolation to zero nonsolvent (20, 25). The data in Table VIII indicated that while the preliminary agreement was not perfect the method has sufficient promise to warrant regular usage. The vistex tech-

TABLE VIII

INTRINSIC FLOW TIME BY VISTEX AND DILUTE SOLUTION TECHNIQUES IN BENZENE

Sample No.	$[t]$, vistex	$[t]$, dilute solution
SM-31-2	0.85	0.85
3	0.84	0.78
4	0.75	0.74
5	0.78	0.72
6	0.81	0.74
SM-33-3	1.85	1.44
4	1.22	1.33
5	1.32	1.31
6	1.55	1.69
SM-34-2	2.22	2.28
3	2.38	2.39
4	2.22	2.34
5	2.36	2.46
6	3.20	3.42
SM-30-3	3.01	3.24
4	3.25	3.50

nique seemed to yield high results for low viscosity polymers and low results for high viscosity polymers relative to the usual dilute solution technique.

Discussion

The system, generally, behaves very similarly to that used for the production of GR–S chemical rubber. The only change in the recipe is the addition of a stabilizing agent, Daxad 11, since during the polymerization the latex particles tend to adhere together or agglomerate, forming prefloc or precoagulum. In this respect the latex has been observed to be quite unstable without this precaution. The rate of the reaction is greater, as can be noted by comparison of the data in Table VII, or Fig. 1, or with similar data obtained at 50° C. (17).

The effect of mercaptan of increasing the rate is well known in the preparation of GR–S (25). Comparison of the regulating index reveals that this is lower for dodecyl mercaptan in the higher styrene ratios than it is for GR–S type copolymers (18, 24). There does not appear to be a waste factor, indeed just the opposite. It is suggested that the increased rate of reaction makes the rate of diffusion of the mercaptan play an increasingly important role until the so-called phase inversion takes place at about 60% conversion. At such a time diffusion no longer is taking place, and particularly with the higher dodecyl mercaptan charges there is an increased rate of disappearance and, in the case of the 30/70 ratio copolymer, a decrease in the viscosity of the polymer found.

The viscosity, unlike that for GR–S (29, 30), does not tend to rise as rapidly, there is less tendency for the pre-gel sharp rise, and when using higher styrene charges and dodecyl mercaptan charges there is indeed no indication of either a rising viscosity or of gel formation up to over 90% conversion. This must be associated with the lower unsaturation of the resin.

The bound styrene data and the values derived from it are more uniform and suggest a system more nearly ideal than that found by Meehan (23). Perhaps the large number of experimental points explains this. In general the data agree well. All suggest that measurements of bound styrene at 60° C. are about 2% absolute high, and allowing for this error the increment styrene curves would be normal. The values for the reactivity ratios are slightly higher than those reported by Meehan (23). No correction was made for bound mercaptan but available data suggest that only a small correction need be made for this.

The calculations of the reactivity ratio in the normal manner yield results that neglect the bifunctional character of butadiene. The correction for this, that is, of assuming each double bond equally reactive, would seem logical at least as a first approximation. The derived values of Q and e agree with experience. The vinyl substituent group is considered to activate the vinyl group as much as, if not more than, does the phenyl group; that is, butadiene double bonds are as reactive as styrene double bonds. On the other hand, the

free radical formed of a butadiene end group is about as active as a styrene one; the growth of a copolymer chain seems to be entirely random.

Acknowledgments

The authors appreciate the courtesy of Polymer Corporation Limited for permission to publish this paper.

The technical assistance of A. Johnston and G. Vincent is gratefully acknowledged.

References

1. AIKEN, W. A. Modern Plastics, 24, No. 6 : 100-102. 1947.
2. ALFREY, T., Jr. and GOLDFINGER, G. J. Chem. Phys. 12 : 205-209. 1944.
3. ALFREY, T. Jr., MAYO, F. R. and WALL, F. T. J. Polymer Sci. 1 : 581. 1946.
4. ALFREY, T., JR. and PRICE, C. C. J. Polymer Sci. 2 : 401-406. 1947.
5. ANON. Modern Plastics, 25, No. 11 : 93-98. 1948.
6. BORDERS, A. M., JUVE, R. O., and HESS, L. D. Ind. Eng. Chem. 38 : 955-958. 1946.
7. BURR, W. Official Digest Federation Paint & Varnish Production Clubs, No. 277 : 198-207. 1948.
8. FORDHAM, J. W. L., O'NEILL, A. N., and WILLIAMS, H. L. Can. J. Research. In press March, 1949.
9. FORDYCE, R. G. India Rubber World, 118 : 377-378. 1948.
10. FORDYCE, R. G., CHAPIN, E. C., and HAM, G. E. J. Am. Chem. Soc. 70 : 2489-2492. 1948.
11. FOX, K. M. India Rubber World, 117 : 487-491. 1948.
12. HARRISON, B. A. and MEINCKE, E. R. Anal. Chem. 20 : 47-48. 1948.
13. HENDERSON, D. A. and LEGGE, N. R. To be published.
14. HOUSTON, R. J. Anal. Chem. 20 : 49-51. 1948.
15. JONES, M. E. and PRATT, D. M. India Rubber World, 117 : 609-610. 1948.
16. KOLTHOFF, I. M. and HARRIS, W. E. Ind. Eng. Chem., Anal. Ed. 18 : 161-162. 1946.
17. KOLTHOFF, I. M. and HARRIS, W. E. J. Polymer Sci. 2 : 41-48. 1947.
18. KOLTHOFF, I. M. and HARRIS, W. E. J. Polymer Sci, 2 : 49-71. 1947.
19. KONRAD, E. and LUDWIG, R. U.S. Patent No. 2,335, 124. Nov. 23, 1943.
20. MAHER, E. D. and DAVIES, T. L. Can. Chem. Process Inds. 30, No. 8 : 43-46. 1946.
21. MAHER, E. D. and DAVIES, T. L. Rubber Age, (N.Y.), 59 : 557-562. 1946.
22. MAYO, F. R. and LEWIS, F. M. J. Am. Chem. Soc. 66 : 1594-1601. 1944.
23. MEEHAN, E. J. J. Polymer Sci. 1 : 318-328. 1946.
24. MORTON, M. and NICHOLLS, R. V. V. Can. J. Research, B, 25 : 159-182. 1947.
25. STARKWEATHER, H. W., BARE, P. O., CARTER, A. S., HILL, F. B., Jr., HURKA, V. R., MIGHTON, C. J., SANDERS, P. A., WALKER, H. W., and YOUKER, M. A. Ind. Eng. Chem. 39 : 210-222. 1947.
26. SUSIE, A. G. and WALD, W. J. Am. Chem. Soc. April, 1948, Abstracts 15 P.
27. THEIS, H. R. and AIKEN, W. A. Rubber Age, (N.Y.), 61 : 51-58. 1947.
28. WALL, F. T. J. Am. Chem. Soc. 63 : 1802-1806. 1941.
29. WALL, F. T. and BESTE, L. R. J. Am. Chem. Soc. 69 : 1761-1764. 1947.
30. WALL, F. T., POWERS, R. W., SANDS, G. D., and STENT, B. S. J. Am. Chem. Soc. 69 : 904–907. 1947.
31. WATERMANN, W. W. and PARKER, P. T. U.S. Patent No. 2, 393, 208. Jan. 15, 1946.
32. WEATHERFORD, J. A. and KNOFF, F. J. India Rubber World, 117 : 743-748. 1948.

A DYNAMOMETER FOR DETERMINING DEPTH OF FREEZING IN FOODS[1]

By H. Tessier[2]

Abstract

A dynamometer, designed to determine depth of freezing in frozen foods, such as meat, poultry, and eggs, measures the force required to drive a pointed rod through a sample of the product.

Introduction

The depth of the frozen portion of some food products is frequently a matter of controversy that is often settled by breaking open some units of the frozen food with an ax, thus destroying those units. Often, the depth of freezing is determined by driving a nail into the product. Lack of resistance to the nail indicates an unfrozen portion. This paper describes a dynamometer that will give a semiquantitative estimate of the depth of freezing in foods.

Description

The dynamometer (Fig. 1) consists of a brass cylinder (*A*) at the lower end of which a chuck (*B*) holds a removable pointed rod (*C*). The upper part of the cylinder is threaded to receive a screw cap (*D*) which clamps down the ringhead (*E*) of a bellows (*F*) against a rubber seal (*G*). A steel rod (*H*) screwed into the lower part of the bellows (*I*) guides a metal ram (*J*). The ram weighs 1 lb. and slides freely over the guide. When this ram is brought down with muscular force against an anvil (*K*), the oil that fills the space between the bellows and the cylinder permits the pressure exerted by the blow to be indicated on a pressure gauge (*L*) connected to the cylinder through a bushing (*M*). To prevent damage to the bellows, a stop (*N*), soldered to a screw cap (*D*) limits the upward movement of the bellows when the ram is pulled up against a nut (*O*) or when the point is pulled out of the sample. For convenience when the instrument is not in use, the guide rod can be unscrewed from the anvil and the pointed rod can also be removed from the chuck.

Procedure

The pointed rod is held against the frozen sample, the ram is gripped firmly with one hand and brought down with force against the anvil until the point penetrates the sample. The pressure at each stroke is noted on the gauge. In a completely frozen sample the pressure required to drive the point into the center of the sample is approximately the same for every stroke, but the

[1] *Manuscript received November 1, 1948.*

Contribution from the Division of Applied Biology, National Research Laboratories, Ottawa. Issued as Paper No. 218 of the Canadian Committee on Food Preservation and as N.R.C. No. 1876.

[2] *Technical Officer, Food Investigations*

pressure required and the depth of penetration at each stroke varies with the temperature and the type of goods. In a partly frozen sample a drop in pressure is noted when the point penetrates into the unfrozen portion. For

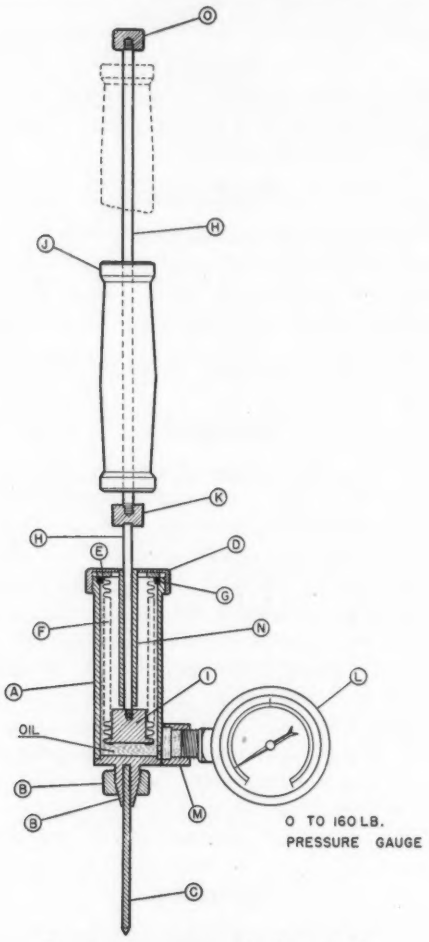

FIG. 1. *Dynamometer for frozen foods.*

example, poultry at 30° F. offers no resistance to the dynamometer, poultry at 20° F. offers about a 50 lb. resistance, and at 0° F. about 160 lb. resistance.

Preliminary trials have indicated that this instrument can be used for inspection work on frozen poultry as a rapid method of detecting unfrozen spots in the center of a carcass. It should be equally useful for determining depth of freezing in other types of frozen flesh, in frozen egg, in fruits frozen in syrup, and in other frozen products.

SOME ELECTROMECHANICAL METHODS FOR PRODUCING LOW FREQUENCIES FROM A PRIMARY FREQUENCY STANDARD[1]

By D. W. R. McKinley[2]

Abstract

Minor mechanical modifications to the clock motor of a quartz crystal primary standard of frequency simplify the problem of producing accurate low frequencies. Electromechanical gate circuits are used to provide pulses of high stability at repetition rates of 1, 10, 100, and 1000 pulses per second for stroboscopic and other applications.

Introduction

The primary standard of frequency at the National Research Laboratories, Ottawa, consists of four temperature-controlled precision quartz crystals and their auxiliary equipment (type C-21-HLD and type 1105-A, General Radio Company). These crystals are checked daily with the official time signals of the Dominion Observatory and with the U.S. Bureau of Standards transmissions. The rates of the crystals are such that a short-term accuracy of 1 part in 10^8 can be guaranteed. The crystal frequency of 50 kc. p.s. is divided by the conventional chain of multivibrators to 10 kc. p.s., 1 kc. p.s., 100 c.p.s., and 10 c.p.s. At the 1 kc.p.s. stage power is furnished to a 1 kc. p.s. phonic motor which rotates at 10 r.p.s. and is geared to drive the hands of a standard clock. There is also a 1 r.p.s. shaft which opens a contactor for about 0.05 sec. each second. This contactor is mounted on a drum, called a microdial, which can be rotated about the shaft to adjust the opening of the contactor to any desired instant in the one-second intervals.

Apart from the standard frequency facilities provided in the spectrum above 50 kc. p.s., which will not be discussed here, the various laboratories require some specific low frequencies for accurate timing applications. The most popular frequency is 60 c.p.s., which unfortunately is incommensurable with the 50 kc. p.s. standard or any of its subharmonics. This 60 c.p.s. frequency was originally obtained by feeding the output of the 10 c.p.s. multivibrator into a double-tripler circuit and filtering the 60 c.p.s. output. The frequency was as accurate as the primary standard when integrated over long periods of time, and was quite satisfactory for clock operation. However, there was a very pronounced jitter of the wave form, due mainly to 10 c.p.s. modulation of the 60 c.p.s. wave, which was never entirely removed even by several sections of filters. This jitter rendered the wave form useless for stroboscopic light devices. Another approach to the problem was more successful. The 1 kc. p.s. output was first tripled to 3 kc. p.s. and then divided by two multivibrator stages to 300 c.p.s. and 60 c.p.s., respectively. The resultant wave

[1] *Manuscript received October 9, 1948.*

Contribution from the Radio and Electrical Engineering Division, National Research Laboratories, Ottawa, Canada. Issued as N.R.C. No. 1869.

[2] *Physicist.*

form was free from subfrequency modulation, and operated stroboscopes more satisfactorily. There was still a noticeable jitter present which was due to the inherent locking instability of multivibrators. Each multivibrator in the chain tends to wander a few electrical degrees about a mean locking position. This type of instability can be minimized by good design but can never be eliminated entirely.

At about this time in the development of the standard frequency services the stroboscope requirements were changed. Instead of 60 c.p.s. it was desired to use short impulses with repetition rates of 1, 10, 100, and 1,000 pulses per second. Although simplifying the situation in one sense this new requirement was not immediately attainable owing to the instabilities of the existing chain of multivibrators. Various other techniques were tried to improve the stability, such as the use of blocking oscillators or regenerative dividers, but none has given as good results with a minimum of equipment as the electromechanical gating system to be described.

FIG. 1. *Schematic diagram.*

Resistances, in thousands of ohms

R1 – 15
R2 – 15
R3 – 15
R4 – 0.3
R5 – 10
R6 – 0.2
R7 – 75
R8 – 25
R9 – 5
R10 – 500
R11 – 75
R12 – 25
R13 – 50
R14 – 10
R15 – 50
R16 – 500
R17 – 0.2
R18 – 75
R19 – 25

Potentiometers, in thousands of ohms

P1 – 50
P2 – 10
P3 – 25

Capacitances, in microfarads

C1	8	electrolytic
C2	0.2	paper
C3	25	electrolytic
C4	8	electrolytic
C5	1	paper
C6	0.01	paper
C7	25	electrolytic
C8	0.1	paper
C9	8	electrolytic
C10	0.01	paper
C11	0.01	paper
C12	25	electrolytic
C13	0.1	paper
C14	0.01	paper
C15	0.001	mica
C16	0.001	mica
C17	0.01	paper
C18	0.0005	mica
C19	25	electrolytic
C20	0.1	paper
C21	0.01	paper

Transformers and Inductances

T1 – Audio interstage, modified as in text
T2 – Audio, 500 ohms to grid
T3 – Audio interstage
L1 – Choke, 30 h.
L2 – 500 ohm winding on permanent magnet
L3 – See L2

Valves

V1 – 6F6, or 6AQ5
V2 – 6AK5
V3 – 1N34
V4 – 6AS6
V5 – 6AL5
V6 – 1N34
V7 – 6AK5

Production of Standard 60 c.p.s. for Clocks

A six-sector disk of 17 gauge Mu metal, 3 in. outside diameter, was mounted on the 10 r.p.s. shaft of the 1 kc. p.s. phonic clock motor. A slot was cut through the laminations of a small high-impedance audio transformer and the transformer mounted so that the sector disk rotated freely through the slot. A few milliamperes of magnetizing current was drawn through one winding of the transformer from the 200 v. d-c. supply for the clock amplifier (See Fig. 1). As the sectors pass through the slot, the flux variations induce a 60 c.p.s. voltage of a trapezoidal wave form in the other winding of the transformer. The wave form is smoothed by a single-section tuned filter, L1, C2 of Fig. 1, and amplified by V1. This 60 c.p.s. sine wave voltage is made available throughout the laboratories. Individual 200-w. amplifiers are installed locally to avoid difficulties with voltage regulation inherent in a common power amplifier. The 60 c.p.s. wave form is satisfactory for clocks and synchronous motors. The simple sector-disk device has eliminated the

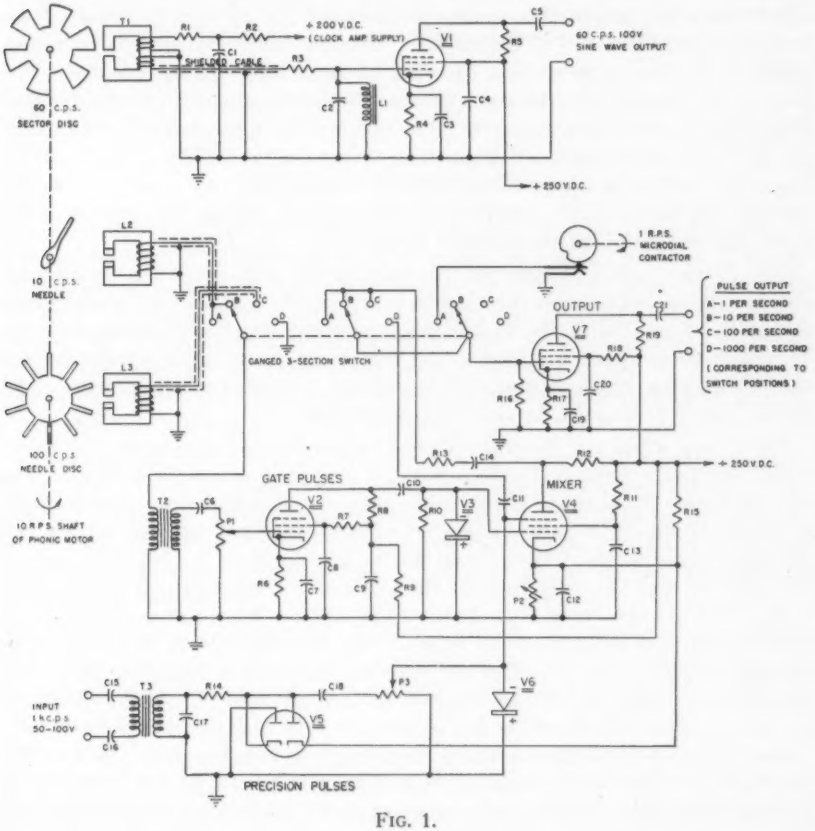

FIG. 1.

10 or 12 vacuum tubes and circuits used in either of the electronic methods described above. The reliability has also improved considerably, because most of the usual faults or failures will affect the amplitude only and not the frequency. This was not always true of the multibrators and other electronic dividers which could sometimes lock on the wrong submultiple after a power-line failure, or run uncontrolled if a circuit failure occurred at an intermediate stage in the chain.

It is true that the phase of the 60 c.p.s. will wander slightly owing to hunting of the 1 kc. p.s. phonic motor. This hunting is usually quite small but can have a maximum amplitude of about $\pm$ 30 electrical degrees at 1 kc. p.s., or about 2 degrees at 60 c.p.s., which is negligible for clock operation although excessive for stroboscopic applications.

Production of Precision Timing Pulses

In addition to the 60 c.p.s. sector disk a narrow strip of 17 gauge Mu metal was also mounted on the 10 r.p.s. shaft of the clock. This strip, or needle, was dynamically balanced to avoid vibration and the tip filed to a square cross section of the thickness of the metal. Another Mu metal disk is provided, which is in effect a small disk carrying 10 accurately spaced needles. The 10 c.p.s. needle and the 100 c.p.s. disk needles each pass through the poles of similar small permanent magnets. The magnets have tapered poles to confine the field to a small angular displacement of the needles. The pickup coils on the magnets have an approximate effective impedance of 500 ohms. Screw-and-slot adjustments are provided for moving the magnets slightly in order to change the phases of the induced voltages.

The voltage pulses induced in the coils by the passage of the needles are not directly usable because they can have a jitter of as much as 80 to 90 μsec., corresponding to the 30 electrical degrees of motor hunting mentioned above. Therefore these pulses are used solely as gate pulses to select, at the desired repetition rate, pulses of much higher timing precision which are produced at the 1 kc. p.s. stage in the counting-down chain.

Fig. 1 is a schematic diagram of the electromechanical system. Suppose, for example, the ganged 3-section selector switch is set at position *B*. The voltage pulses from the 10 c.p.s. needle pickup coil, which have a wave form as shown in Fig. 2 (*a*), are differentiated, amplified, and squared by V2 and its associated circuits. The crystal diode, V3, removes the negative part of the wave so that the wave form at the input to the control grid of the mixer valve V4 is as shown in Fig. 2 (*b*). The dotted wave forms of Fig. 2 (*b*) indicate the probable amount of jitter. The precision timing pulses are then derived from the 1 kc. p.s. clock amplifier by means of the clipping valve, V5, the differentiating circuit, C18, P3, and the crystal diode, V6. The constants of these circuits have been chosen to produce 1 kc. p.s. positive pulses at the suppressor grid of V4 with a sharp rising edge and an approximate duration of 100 μsec. The wave form of these pulses is shown in Fig. 2 (*c*). The cathode bias of V4 is adjusted by means of P2 so that no anode current is

drawn if either the 1 kc. p.s. pulses or the gate pulses are applied separately to the grids of V4. (Incidentally, this positive bias voltage also sets the clipping level of the 1 kc. p.s. pulses.) However, if both the gate pulse and a

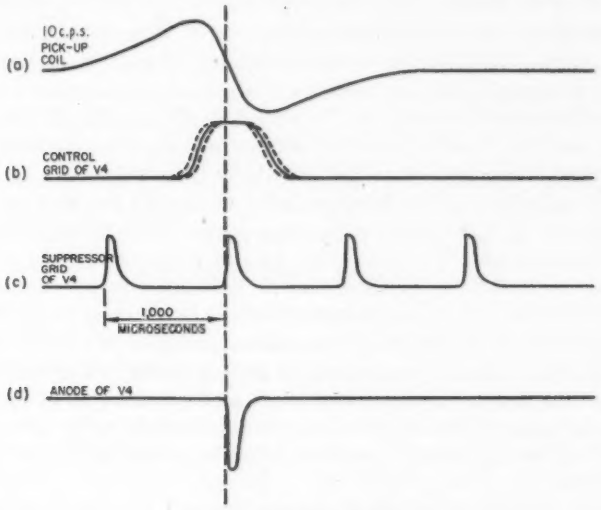

FIG. 2. *Voltage wave forms.*

1 kc. p.s. precision pulse are applied coincidentally to V4, anode current will flow and an anode pulse is produced as shown in Fig. 2 (*d*). The phase of the gate pulse is adjusted mechanically to ensure that the gate will straddle the precision pulse. The output of V4 is then amplified by V7 to about 100 peak volts. Thus the output pulses are actually the same pulses as supplied to the suppressor grid of V4 but selected at a rate of 1 in 100, or 10 per sec. The timing precision of these pulses is the same as that of the original 1 kc. p.s. source and is not affected by jitter of the gate pulse.

If the selector switch is now set to position *A* the microdial contactor will ground the grid of V7 except over a period of approximately 0.05 sec. each second. This gate, which is considerably wider than a single pulse but not wide enough to include two 10 c.p.s. pulses, can be phased by the microdial to straddle one of the output pulses. The over-all rate is now 1 in 1000 or one pulse per second.

Putting the selector switch on position *C* simply connects the input of V2 to the 100 c.p.s. needle disk. The operation is the same as described above for position *B* except that the output pulses are now selected at the rate of 1 in 10 or 100 pulses per second.

When the selector switch is in position *D* the mixer tube V4 is by-passed and the precision pulses are supplied directly to the output stage at a rate of 1000 pulses per second. The output pulses in this case will be negative,

whereas the pulses produced at switch positions *A*, *B*, and *C*, are positive, owing to the inversion occurring in V4. A single triode push-pull inverter stage could be added to the output to provide low-impedance positive or negative pulses as desired, but this feature was not required in the laboratory.

When examined on a high-speed osilloscope it is seen that the 1 kc. p.s. precision pulses produced from the 1 kc. p.s. standard frequency source actually have a small jitter of the order of a microsecond or less, representing an interval timing error of one part in a million at one pulse per second. The uncertainty in the triggering of stroboscope tubes is rather greater than this, so the stability of the pulse is fully adequate for these purposes. This residual jitter is attributable to the characteristics of the 10 kc. p.s. and 1 kc.p.s. multivibrators. If it is desired to produce pulses at low repetition rates with jitters of the order of 0.1 or even 0.01 μsec. it will be necessary to form the pulses at the crystal frequency and then to gate these pulses electronically at 10 kc. p.s. and 1 kc. p.s. For example, this can be done by using the existing multivibrators solely to provide gating pulses to mixer circuits, similar to that shown in Fig. 1, at the 10 kc. p.s. and 1 kc. p.s. levels. The resultant pulse produced at the one pulse per second level, say, will have an extremely small jitter but the pulse will necessarily be quite short, of the order of 1 or 2 μsec., and some lengthening may be required to make it usable in practical timing applications.

The electromechanical gating technique described above is applicable to any of the usual types of quartz crystal primary or secondary standards incorporating an electric clock at some stage in the frequency division chain, and it offers several advantages over purely electronic methods below 1 kc. p.s. in simplicity of apparatus, reliability of operation and maintenance of precision.

Acknowledgment

Mr. W. E. M. Dale built and installed the circuit elements, and the mechanical parts were prepared by the staff of the machine shop under Mr. I. L. Newton.

OBSERVATIONS ON THE ADSORPTION OF WATER VAPOR BY WHEAT[1]

By J. D. Babbitt[2]

Abstract

The adsorption and desorption of water vapor by wheat was measured by means of a McBain sorption balance. Curves are obtained showing the rate at which moisture is adsorbed by kernels of wheat directly exposed to a humidified atmosphere, and a theory is advanced to account for the rate of adsorption. It is shown that the rate of adsorption is governed largely by the time taken for the moisture to diffuse up to the surface of the wheat. Under storage conditions, this is much greater than the time required for the moisture to penetrate the kernel of wheat from its surface.

The Adsorption Isotherm

Several observers (4, 6, 7) have measured the water vapor adsorption isotherm for wheat, but no provision was made in any of the measurements to distinguish between adsorption and desorption and no measurements were recorded on wheat of low moisture content. In order to study the difference between adsorption and desorption and to observe the behavior at low moisture contents some measurements were made with wheat by means of a McBain sorption balance. Preliminary results have already been published (2) but more extensive data are now available and are worth recording.

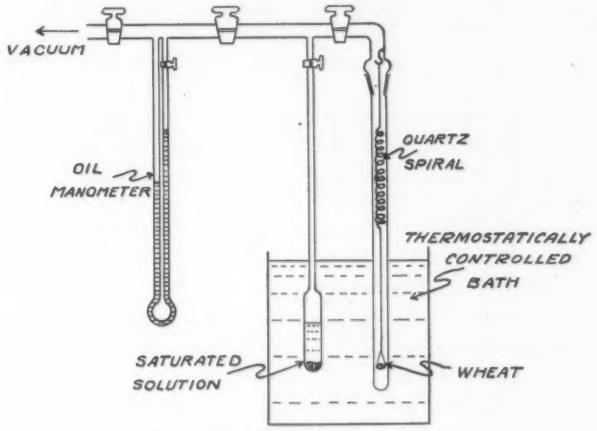

Fig. 1. *Adsorption apparatus.*

The arrangement of the apparatus is shown in Fig. 1. The wheat (approximately 10 kernels) was suspended on a quartz spiral in a glass tube. A

Manuscript received September 27, 1948.

Contribution from the Division of Physics, National Research Laboratories, Ottawa, Canada. Issued as N.R.C. No. 1882.

[2] *Physicist.*

saturated salt solution, held at a constant temperature by the same water bath that surrounds the wheat, maintained a constant relative humidity in the glass tube, and various humidities were obtained by using different salts. The air was evacuated from the system so that all measurements were made in an atmosphere of water vapor alone. The vapor pressure was measured by means of a manometer containing a vacuum oil having a low vapor pressure. The extension of the spiral spring was measured with a cathetometer and the spring was calibrated by the use of standard weights.

To determine an isotherm, the wheat, which had been previously dried, was placed on the balance and the apparatus evacuated. The extension of the spring, as then measured, corresponded to the dry weight of the wheat. The system was then opened to the saturated solution and the extension of the spring measured at intervals until there was no further elongation. At the same time the pressure as given by the manometer was recorded. In some observations, measurements were continued over several days in order to be certain that the adsorption was complete. The moisture content was calculated from the extension of the spring, and the vapor pressure was obtained from the manometer reading. When an observation at one relative humidity was completed, the solution was changed and the procedure repeated. In this way the complete isotherm was obtained.

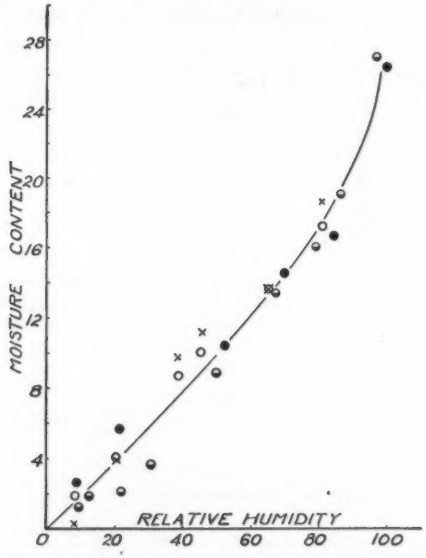

FIG. 2. *Adsorption isotherm. 25° C.*

The results of the measurements on adsorption are collected in Fig. 2 while those for desorption are given in Fig. 3. Throughout this paper the moisture content is expressed as percentage of the dry weight of the wheat.

The wheat used was, in one experiment, No. 1 Northern Garnet wheat and in the others No. 1 Northern Marquis wheat. It was not intended in these experiments to study the difference in behavior of various varieties of wheat but only to observe the general nature of the adsorption.

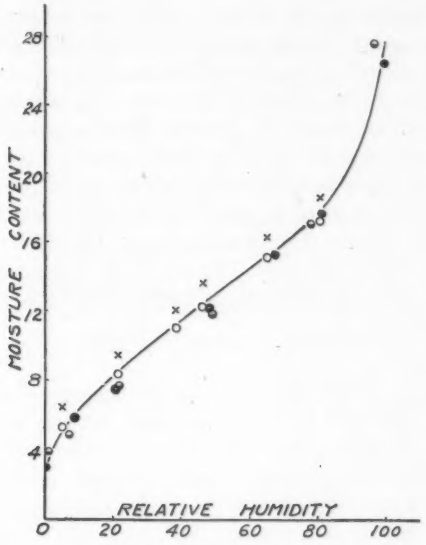

FIG. 3. *Desorption isotherm.*

For both adsorption and desorption there is considerable scatter in the results, but it should be noted that for a series of readings on any one sample the points for desorption appear to give a more consistent curve than those for adsorption; for any one series of points in Fig. 3 a smooth sigmoid curve is obtained but for adsorption this is not so. In Fig. 2 the experimental points are scattered uniformly about a mean curve and each series of measurements does not have the continuity that is found in desorption.

At low moisture contents the curve for adsorption is convex to the humidity axis and there is no indication of the concave curvature that is often found for adsorption by organic materials and that is clearly shown in the desorption curve. One set of measurements (represented by •) does indicate such a curvature but this is not substantiated by the other measurements. The individual points for desorption for each sample of wheat lie on a fairly smooth curve although the curves for different samples do not exactly coincide. There is no doubt that the desorption curves have a definite reversal of curvature and are strongly concave to the relative humidity axis at low moisture contents.

It is difficult to say why the behavior of the wheat should differ in this way during adsorption and desorption. The deviation of the individual points

from a smooth curve could have been caused by fluctuations in the vapor pressure; small variations in the temperature of those parts of the apparatus not in the thermostat, or failure of the solution to attain uniform saturation, might change the vapor pressure over a short interval of time sufficiently to give an altered moisture content and, owing to hysteresis, this spurious moisture content would remain when conditions became normal. That this should have occurred during adsorption and not during desorption is improbable. There are other reasons to believe, moreover, that these differences are not the result of fluctuations in the vapor pressure; in several of the experiments two balances were used and yet there was no correlation in the deviations for two samples of wheat even when exposed to the same atmosphere of vapor. Also, in an experiment in which wheat was exposed on one balance and flour on the other, it was found that deviations that occurred for the wheat did not occur for the flour. The measurements made on a sample of flour are shown in Fig. 4. It should be noted that the hysteresis is less pronounced than for wheat and the curve for adsorption is concave to the humidity axis at low moisture contents.

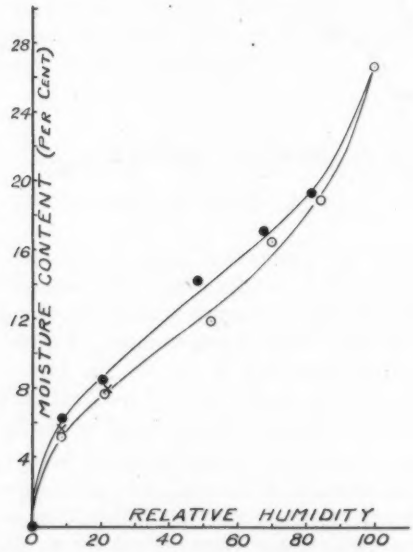

FIG. 4. *Adsorption by flour.* ⊙ *Adsorption.* ● *Desorption.* × *Second adsorption.*

With the exception of one run at 34° C. (Fig. 5) the experiments were carried out at a temperature of 25° C. At 34° C. it was impossible to take the measurements to high relative humidities, as under these conditions condensation occurred in the parts of the apparatus that were at room temperature.

In completing the desorption curve it was never possible to remove all the moisture from the wheat. To obtain zero relative humidity, the apparatus

was evacuated with a mercury diffusion pump. After days of evacuation the wheat still retained several per cent of moisture and no appreciable change of moisture content occurred from one day to the next. This residual moisture

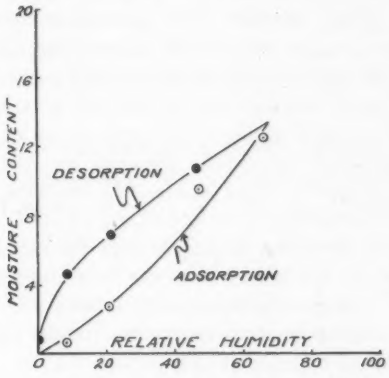

FIG. 5. *Isotherm for wheat at 34° C.*

content is shown graphically by the fact that in Fig. 3 the desorption curve for 25° C. cuts the axis at approximately 3% moisture content. The effect for the curve at 34° C. is less pronounced; throughout its length the desorption branch is below that for 25° C. and the residual moisture content is only 0.8%. Thus it is evident that the residual moisture content is a function of temperature. With the flour the moisture was completely removed by evacuation.

There was some question whether this residual moisture content was real; the difference between the final and original weight might represent an addition to the dry weight of the wheat caused by the cycle of moisture changes to which it had been exposed. That it was a true residual moisture content was shown by the following. A sample of wheat that had undergone a desorption cycle and after evacuation had retained some residual moisture was exposed to an increasing series of relative humidities so that a second adsorption curve was obtained. When the relative humidity had increased to 20% the moisture content was equal to that obtained in the original adsorption measurements. An additional proof is given by the fact that the wheat when removed from the apparatus and dried to constant weight in a vacuum oven had the original dry weight.

The Time-Rate of Change of Moisture Content

Introduction

The time required for the moisture content of wheat to come to equilibrium with any relative humidity to which it is exposed is not only of scientific interest but also, owing to the influence of moisture content on the keeping quality of wheat, of great commercial importance. Many factors influence

the rate at which water vapor is adsorbed by wheat and this is especially true when the kernels are not isolated but are confined within the bulk of a mass of wheat. It is obvious that a single kernel of wheat directly exposed to water vapor will take up moisture more quickly than kernels several inches below the surface in a grain elevator. On account of the resistance of air to the movement of water vapor one would expect that the rate of approach to equilibrium would be slower in air than in an atmosphere having the same water vapor pressure but from which the air has been exhausted. If, however, the air is maintained in rapid motion the water vapor at the surface of the kernel will be replenished as fast as it is adsorbed and the rate of adsorption will more nearly equal that of vapor alone. In studying the rate at which moisture is taken up by wheat it is important to distinguish between the effect of the diffusion of the water vapor through the air and the surrounding wheat up to the surface of the kernel from the diffusion through the skin and into the kernel itself. Before describing some experiments that were devised to disentangle these effects it is necessary to discuss the fundamentals of diffusion theory.

Fundamentals of Diffusion

If the coefficient of diffusion is defined as the ratio of the total mass that flows across unit area of any small section in unit time to the rate of decrease of density per unit distance in a direction perpendicular to that section, the fundamental equation of diffusion is

$$\frac{dQ}{dt} = -D\frac{d\rho}{dx}\,dydz\,, \tag{1}$$

where dQ is the mass passing through a plane of area $dydz$ in time dt, D is the coefficient of diffusion, and $\frac{d\rho}{dx}$ the density gradient.

From this fundamental equation, the differential equation governing diffusion (Fick's law) may be derived in a manner similar to that by which Fourier's equation is obtained in the analogous phenomenon of heat flow. We consider the flow of matter into and out of a differential block through the two faces normal to the direction of the x-axis, and obtain

$$\left(\frac{\partial Q}{\partial t}\right)_x = -\left(D - \frac{1}{2}\frac{\partial D}{\partial x}\,dx\right)\frac{\partial}{\partial x}\left(\rho - \frac{1}{2}\frac{\partial \rho}{\partial x}\,dx\right)dy\,dz + \left(D + \frac{1}{2}\frac{\partial D}{\partial x}\,dx\right)\frac{\partial}{\partial x}\left(\rho + \frac{1}{2}\frac{\partial \rho}{\partial x}\,dx\right)dy\,dz$$

$$= \left(D\frac{\partial^2\rho}{\partial x^2} + \frac{\partial D}{\partial x}\frac{\partial \rho}{\partial x}\right)dx\,dy\,dz\,.$$

But since $\left(\frac{\partial Q}{\partial t}\right)_x = \left(\frac{\partial \rho}{\partial t}\right)_x dx\,dy\,dz$

$$\left(\frac{\partial \rho}{\partial t}\right)_x = D\frac{\partial^2\rho}{\partial x^2} + \frac{\partial D}{\partial x}\cdot\frac{\partial \rho}{\partial x}$$

$$= D\frac{\partial^2\rho}{\partial x^2} + \frac{\partial D}{\partial \rho}\cdot\frac{\partial \rho}{\partial x}\cdot\frac{\partial \rho}{\partial x}$$

$$= D\frac{\partial^2\rho}{\partial x^2} + \frac{\partial D}{\partial \rho}\cdot\left(\frac{\partial \rho}{\partial x}\right)^2 - - - . \tag{2}$$

By similar considerations in the y and z directions we get for the equation in three dimensions

$$\frac{\partial \rho}{\partial t} = D \nabla^2 \rho + \frac{\partial D}{\partial \rho} (\text{grad } \rho)^2 . \tag{3}$$

This is the exact differential form of Fick's law. If D is independent of the concentration the second term is zero and we have the simple form which has been solved for most of the common geometrical shapes and is, therefore, generally used.

In experimental work on gases, the pressure, rather than the concentration, is measured and quite commonly the diffusion coefficient is expressed as the mass flow per unit pressure gradient. For gases in free space, where the concentration is linearly proportional to the pressure, the use of the pressure rather than the concentration gradient is equivalent to multiplying D by a constant factor. When, however, we come to study the diffusion of gases through solids the pressure is not always proportional to the density, for all the complications associated with adsorption are present; it is exceedingly rare to find any substances for which the amount of material adsorbed is linearly proportional to the pressure, and before applying the pressure gradient to the diffusion equation it is necessary to develop the appropriate equation from fundamentals.

We start by writing the fundamental Equation (1) in terms of a second diffusion coefficient D_p, which bears to the pressure gradient the same relation that D bears to the concentration gradient.

$$\frac{dQ}{dt} = - D_p \frac{dp}{dx} dy\, dz , \tag{4}$$

and proceeding as before we develop the differential equation in terms of the pressure.

$$\left(\frac{\partial \rho}{\partial t}\right)_x = D_p \frac{\partial^2 p}{\partial x^2} + \frac{\partial D_p}{\partial p} \left(\frac{dp}{dx}\right)^2 . \tag{5}$$

This may be written

$$\frac{\partial \rho}{\partial p} \left(\frac{\partial p}{\partial t}\right)_x = D_p \frac{\partial^2 p}{\partial x^2} + \frac{\partial D_p}{\partial p} \left(\frac{\partial p}{\partial x}\right)^2 . \tag{6}$$

In considering the diffusion of a gas such as water vapor through an adsorbing material such as wheat the concentration ρ would be the weight of water vapor per unit volume. In adsorption, however, the moisture content is commonly expressed as the weight adsorbed per unit weight of dry adsorbent. If m is the moisture content and μ the density of the dry adsorbent we have

$$\rho = m \mu ,$$

and

$$\frac{\partial \rho}{\partial p} = \mu \frac{\partial m}{\partial p} .$$

Now $\frac{\partial m}{\partial p}$ is the slope of the adsorption isotherm and following Daynes (5) we shall call it the specific solubility and denote it by S. Then

$$\frac{\partial \rho}{\partial p} = \mu S , \tag{7}$$

and Fick's law has the form

$$\mu S \left(\frac{\partial p}{\partial t}\right)_z = D_p \frac{\partial^2 p}{\partial x^2} + \frac{\partial D_p}{\partial p}\left(\frac{\partial p}{\partial x}\right)^2 . \tag{8}$$

In three dimensions

$$\mu S \frac{\partial p}{\partial t} = D_p \nabla^2 p + \frac{\partial D_p}{\partial p} (\text{grad } p)^2 \tag{9}$$

In order to find the relation between the two coefficients D and D_p we take the two fundamental equations

$$\frac{dQ}{dt} = - D \frac{d\rho}{dx} dy\, dz$$

and

$$\frac{dQ}{dt} = - D_p \frac{dp}{dx} dy\, dz .$$

If $\frac{dQ}{dt}$ is the same in both equations we must have

$$D \frac{d\rho}{dx} = D_p \frac{dp}{dx} ,$$

and

$$D_p = D \frac{d\rho}{dp}$$

$$= D \mu S . \tag{10}$$

We have already mentioned the analogy between the equations of diffusion and those of thermal conductivity; Equation (10) is analogous to the relation between the thermal conductivity k and the thermal diffusivity κ. In Fourier's equation we find

$$\kappa = \frac{k}{dc} ,$$

where d is the density and c the specific heat. It is evident, therefore, that D corresponds to the thermal diffusivity, D_p to the thermal conductivity, and S to the specific heat. The pressure p is the potential function corresponding to the temperature.

Rate of Approach to Equilibrium in Wheat

The movement of water vapor into wheat can be studied by exposing wheat to an atmosphere of constant relative humidity and measuring the change of weight with time. With this idea in mind several different types of experiments were carried out. In some a small quantity of wheat was placed in a weighing bottle and exposed in a desiccator to an atmosphere of constant humidity; in other experiments the weighing bottle with the wheat was exposed in a small chamber, which was maintained at constant temperature and humidity and in which the air was rapidly circulated by means of a

fan; in one single experiment the approach to equilibrium was measured on one of the sorption balances used in the experiments described in the first part of this paper. In all experiments, saturated salt solutions were used to obtain a constant humidity, and sodium chloride, which gives a relative humidity of 75%, was the solution employed in the majority of the experiments.

As previously mentioned there are two aspects of adsorption that must be considered; first, there is the diffusion of the water vapor from the solution to the surface of the wheat and, secondly, there is the diffusion through the skin and into the kernel. The preliminary experiments were designed to eliminate the effect of diffusion through the air and to obtain as closely as possible an estimate of the time required for the moisture to penetrate the kernel from its surface. The wheat was, therefore, exposed in a single layer so that no superimposing wheat was present to restrict the movement of the moisture up to the wheat.

The results obtained from some of the experiments with single layers of wheat are reproduced in Fig. 6. The curves in this graph show that the

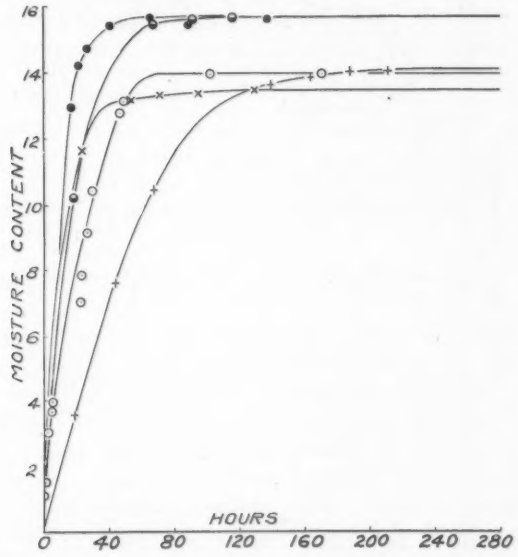

FIG. 6. *Rate at which moisture is adsorbed by single layers of wheat under various conditions.* ⊙ *Sorption balance in vacuum.* × *Humidity chamber with fan.* ● *Humidity chamber with fan.* ◒ *Humidity chamber with fan.* + *Desiccator.*

moisture content increased most rapidly for the wheat that was exposed in the humidity chamber with a fan blowing the air over the surface of the kernels, and least rapidly for the wheat in the desiccator. The wheat on the sorption balance adsorbed the moisture at a rate slightly less than that in

the humidity chamber; one might have expected the adsorption on the balance to proceed more quickly since it took place in an atmosphere of water vapor with no air present to resist the movement of the moisture. There was, however, considerable glass tubing between the solution and the wheat, and this may have substantially delayed the movement of the moisture. The evaporation of the moisture from the surface of the solution may also have been slower in this apparatus since in the humidity chamber the air was directed across the surface of the solution by the fan. The final equilibrium value was not the same in all these experiments, owing to differences in the wheat or variations in the relative humidity, but nevertheless the differences in the rate of approach to equilibrium are obvious.

From these experiments we are entitled to assume that in the humidity chamber the time required for the wheat to reach the equilibrium moisture content is almost completely the result of the resistance to diffusion within the grain itself; that is, we can assume that the rapid circulation of air ensures that at the surface of the wheat the air will contain water vapor in the concentration corresponding to the equilibrium conditions.

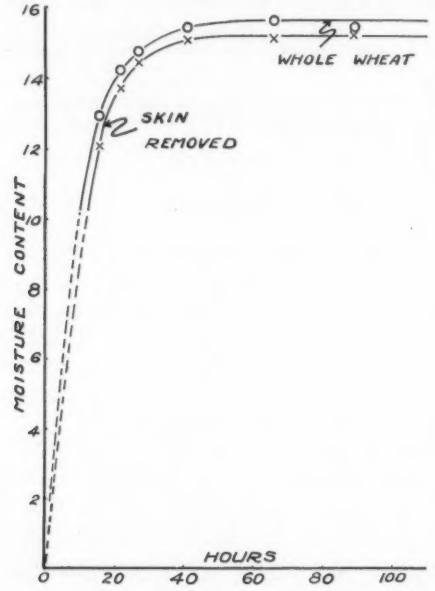

FIG. 7. *Comparison of adsorption by wheat with and without skin.*

As a preliminary consideration it would be natural to assume that the greater part of the resistance to the movement of moisture into the grain resided in its skin (pericarp). In order to test this assumption the skin was removed from several kernels and these were exposed to a moist atmosphere under similar conditions to some whole grains. The results are shown in

Fig. 7. Allowing for the fact that there is a slight difference in the final equilibrium moisture content, the approach to equilibrium is almost identical. The indication is that the skin offers little resistance to the movement of moisture.

Calculation of Rate of Approach to Equilibrium

If we assume that a kernel of wheat is a sphere of homogeneous material and that, under the driving force of the concentration gradient, the moisture diffuses into the sphere according to Fick's law we can calculate the shape of the moisture content versus time curve. Thus if C_0 is the initial concentration in a sphere and C_2 the concentration at the surface, the amount Q_t that has diffused into the sphere in time t is given by

$$Q_t = -(C_2 - C_0)\frac{4\pi a^3}{3}\left[1 - \frac{6}{\pi^2}\sum_1^\infty \frac{1}{n^2} e^{-D\frac{n^2\pi^2 t}{a^2}}\right], \qquad (11)$$

where a is the radius of the sphere. (For derivation of this formula see: "Diffusion in and Through Solids," by R. M. Barrer; Cambridge University Press, 1941, page 29. In this book there is a mistake in the constant.) This equation has been derived from the concentration form of Fick's law and the coefficient D is the true diffusion constant. D has the dimensions of L^2/T.

To adapt this equation for our purpose we replace the concentrations with the corresponding moisture contents and put $Q_t = \frac{4\pi a^3 m}{3}$, where m is the average moisture content throughout the kernel at the time t. For convenience we write $D\frac{\pi^2}{a^2} = D'$. We assume that $m_0 = 0$ and that the moisture content m_2 at the surface of the sphere is the same as the final moisture content. Then we have

$$m = m_2\left[1 - \frac{6}{\pi^2}\left(e^{-D't} + \frac{1}{4}e^{-4D't} + \frac{1}{9}e^{-9D't} + \ldots.\right)\right]. \qquad (12)$$

To test this equation we use the curve for wheat in the humidity chamber with the fan blowing. We evaluate D' by taking the point $t = 20$ hr., $m = 14.00$, and obtain $D' = 0.087$. Using this value of D' we can calculate the whole curve. This is shown in Fig. 8; the fit with the observed results is fairly good but although the curves are similar in shape there are indications that the observed values rise more slowly at the beginning and more rapidly at the end than the calculated values. The calculated values are based on a diffusion coefficient D which remains constant throughout the adsorption; the observed results indicate that D increases as the moisture content of the grain increases.

Several workers have pointed out that at low moisture contents vapors diffuse through adsorbing materials much more slowly than at high moisture contents. In addition there is a secondary effect that may exert considerable influence on the adsorption. We have shown in Equation (10) that the concentration coefficient is related to the pressure coefficient by the relation

$D = D_p/\mu S$ and is thus inversely proportional to the specific solubility S. The specific solubility, which is the slope of the adsorption isotherm, increases with humidity, as is clearly shown in Fig. 2. As S increases, the

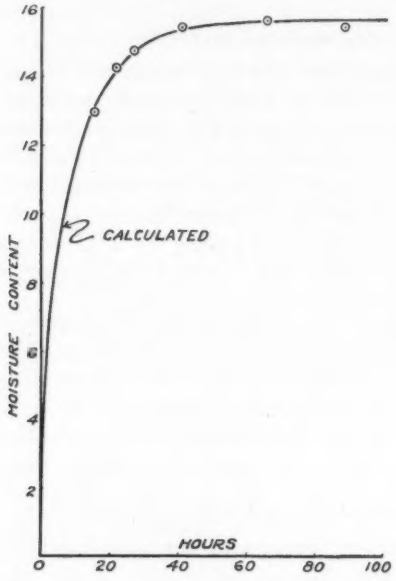

FIG. 8. *Comparison of calculated with observed rate of adsorption.* ⊙ *Observed.*

diffusion coefficient D should decrease. Since experimentally we find that, during adsorption, D actually seems to increase we can only infer that the effect of the specific solubility S is masked by a greater change in the coefficient D_p.

When we study the drying of wheat, the effect of the variation in the coefficient is more pronounced. To study this, the process described above was reversed; wheat having a moisture content around 15% was exposed to a dry atmosphere. In all but one of these desorption experiments the wheat was exposed in a desiccator and the air was still. In one experiment the desiccator was evacuated. Although we have already seen from Fig. 6 that the exchange of moisture is considerably delayed by the resistance of the air yet by comparing the desorption with adsorption under similar conditions we can readily see the differences in the two processes.

In Fig. 9 the results of two desorption experiments with single layers of wheat are shown and two adsorption curves have been reproduced for comparison. There are two important factors that distinguish the desorption from the adsorption curves; the desorption curves do not reach an end point and there appears to be a residual moisture content that would not be removed even after an infinite length of time. One of the desorption curves was

obtained with the wheat in an evacuated desiccator and the other with the wheat in a desiccator at atmospheric pressure. There is little difference in the rate of desorption and the difference that is shown may well be explained

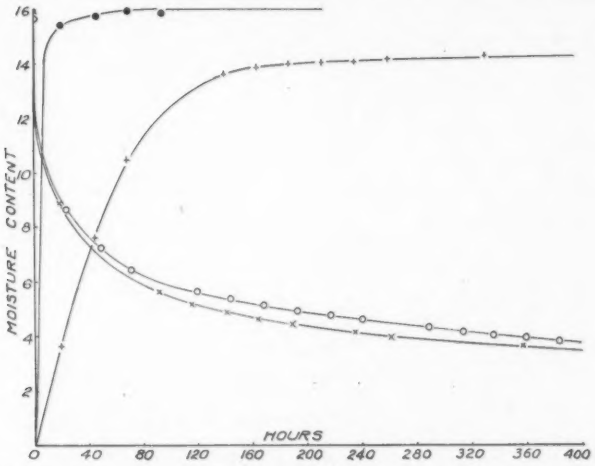

FIG. 9. *Comparison between adsorption and desorption.* ○ *Desorption in vacuum desiccator at room temperature.* × *Desorption in desiccator at 91.3° C.* ● *Adsorption in humidity chamber with fan.* + *Adsorption in desiccator.*

by a difference in temperature. The desorption in the evacuated desiccator should be comparable to the adsorption under the most rapid conditions, and a curve showing the adsorption with a fan blowing a current of air across the wheat is reproduced. The second adsorption curve was obtained with the wheat in a desiccator containing a saturated sodium chloride solution under still air conditions. In the initial stages there is some resemblance between this adsorption curve and the desorption curves but the adsorption curve, and this occurs in all experiments, does come to a definite end point. The difference in the shape of the adsorption curve obtained with the air in rapid motion is most pronounced. There the adsorption rises rapidly and decisively to an end point.

The fact that it is impossible to remove all the moisture from wheat at room temperatures by evacuation or desiccation has already been noticed in the experiments with the sorption balance. There it was also found that if the temperature was raised the residual moisture content was lowered. To elucidate this point, desorption curves were obtained at higher temperatures. These are shown in Fig. 10. The curves were obtained with wheat under atmospheric pressure in a desiccator. The effect of increase of temperature is readily apparent, the initial loss of moisture being more rapid and the final values lower. In all curves there is still a finite decrease in the moisture content at the conclusion of the experiments. It is impossible to say whether this decrease would go on indefinitely and whether the wheat would finally

attain zero moisture content. It is evident, however, that at some temperature (perhaps the boiling point of water) all the water vapor would be removed; this is a basic assumption in this work, as the final weight obtained in a vacuum oven has been taken as the dry weight of the wheat.

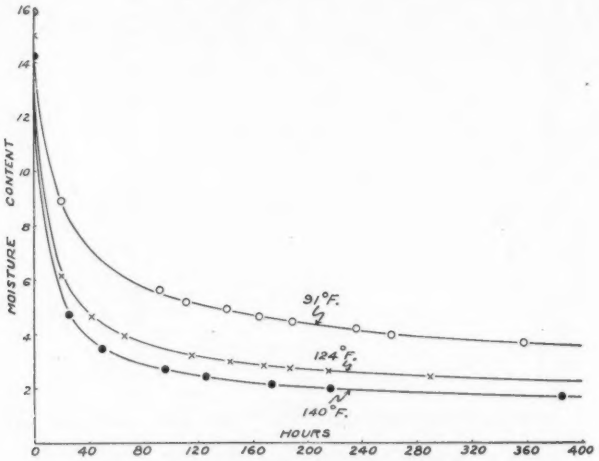

FIG. 10. *Effect of temperature on desorption.*

The difference in the behavior of the wheat during adsorption and desorption might have been forecast from the differences in the adsorption and desorption isotherms. We have pointed out that the diffusion coefficient D is equal to $\frac{D_p}{\mu S}$ and is therefore inversely proportional to the specific solubility. In the desorption curves, on account of the reverse curvature, the slope is very large at low moisture contents and becomes infinite as we approach the origin. D, therefore, becomes small and the desorption would proceed very slowly. The behavior of D during desorption can be seen more clearly if we attempt to fit the experimental curve with Equation (12). For desorption this has the form

$$m = m_0 - (m_0 - m_2)\left[1 - \frac{6}{\pi^2}\sum_1^\infty \frac{1}{n^2}\, e^{-n^2 D' t}\right], \qquad (13)$$

in which m_0 is the initial and m_2 the final moisture content. Since the end point is not zero we have to assume an appropriate value for m_2.

The values calculated from this equation for the curve at 91.3° F. are shown in Fig. 11; $m_0 = 15.90$, $m_2 = 3.40$, and D' was found to be equal to 0.014. To determine D' the calculated values were made to fit the experimental values at $t = 100$. It is immediately seen that the desorption is more rapid at the beginning and less rapid at the end than that given by the equation. It should also be noted that the equation gives a constant value for the moisture content after 400 hr., while the experimental results are

still decreasing at this point and give no indication of reaching an equilibrium value. The difference between the calculated curve and the experimental points is strong evidence that D' is decreasing throughout the experiment.

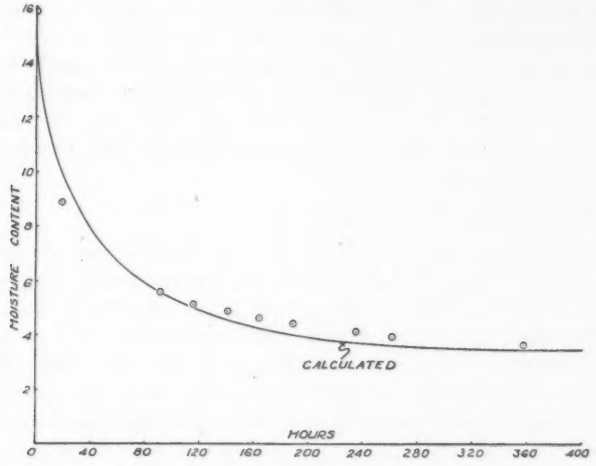

FIG. 11. *Relation between observed and calculated values for desorption.* ⊙ *Observed values.*

We have stated that the low value of D' at low moisture contents is the reason for the slow approach to equilibrium. This low value of D' results from the high curvature of the desorption curve near the origin. In order to

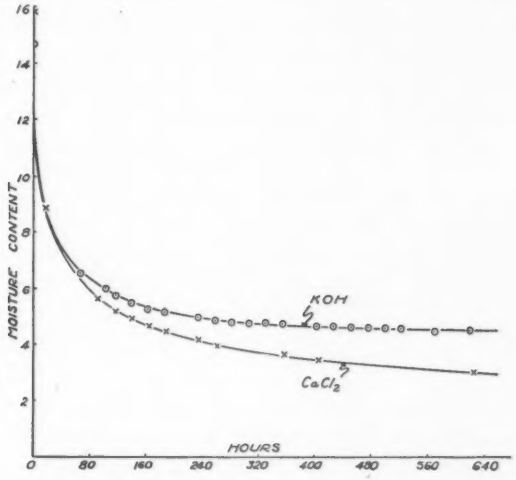

FIG. 12. *Difference in desorption with potassium hydroxide and calcium chloride.*

show the effect of this, two desorption experiments were made under similar conditions, in one of which the desiccant was calcium chloride and in the other potassium hydroxide. Potassium hydroxide gives a relative humidity of approximately 9% and, according to Fig. 3, the specific solubility would be finite in that region. We should expect the moisture in the wheat exposed to potassium hydroxide to reach a definite end point, in contrast to the behavior usual with calcium chloride. That such is the result is shown in Fig. 12. The desorption with potassium hydroxide, while proceeding at the beginning at a rate not much slower than that with the calcium chloride, does appear to have reached an end point at 600 hr., while the other curve gives no such indication.

Experiments on Adsorption in Depth

It has already been pointed out that when wheat is present in bulk one would expect that kernels in layers below the surface would pick up moisture much more slowly than those on the surface, and that consequently dry wheat exposed to humidity would not attain equilibrium throughout its depth for a considerable length of time. Some evidence of this effect has already been shown by the difference in the time required for wheat to adsorb moisture when exposed in still air in contrast to a vacuum or rapidly moving air. One would expect the presence of other wheat kernels, which makes it necessary for the moisture to diffuse through the interstices between the grains, to increase this effect and to reduce the rate of adsorption to a very low value. That such is the result is shown by some simple experiments.

Small samples of wheat were placed in cylindrical glass vessels approximately $1\frac{1}{2}$ in. in diameter. The height of the vessels and the depth of the wheat varied in the different experiments. In a constant-temperature chamber, the samples were exposed at the top surface to a constant relative humidity of 75% with a fan blowing over the surface of the wheat.

The results are shown in Fig. 13. The measurements were made for a period of 400 hr. The abscissae are the amounts of moisture adsorbed expressed as a percentage of the total weight of wheat. As the depth of the wheat becomes greater the percentage of moisture adsorbed during any period becomes smaller. It is obvious that the adsorption would not be uniform throughout the wheat but that the kernels on the surface would be close to the equilibrium value, while those deep in the vessel would have taken up a very small amount of moisture. If the experiments were carried on for a sufficient length of time all the wheat throughout the vessel would ultimately arrive at the equilibrium moisture content, and the rate at which it approaches equilibrium gives a measure of the slowness of diffusion through wheat.

It is evident from these curves that water vapor can move through wheat only very slowly. Even so little as an inch of wheat has retarded the adsorption to such an extent that the process is only just complete at the end of 400 hr. With a depth of 6 in. the process is only a third completed at the

end of this period and, since the rate of the process gets progressively slower as equilibrium is approached, it is obvious that it would require a very long period indeed before the whole of the wheat had reached the equilibrium moisture content.

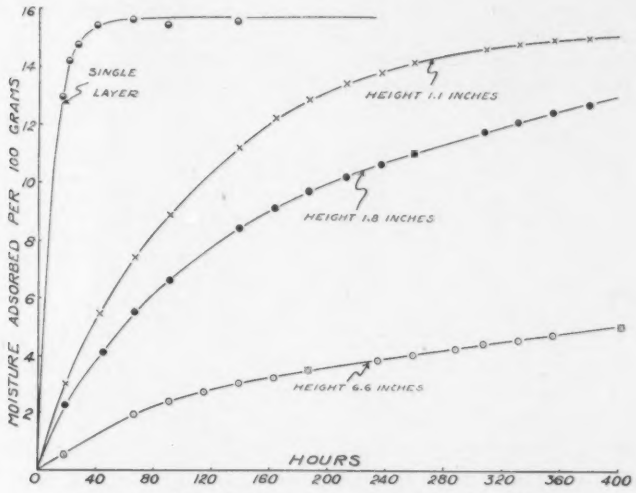

FIG. 13. *Effect of depth of wheat on rate of adsorption.*

These simple experiments give some idea of the length of time that is necessary before moisture from the atmosphere can penetrate into a mass of wheat. It is obvious that in any reasonable time only the surface layers of the wheat will be affected. Were this not so, wheat could not be stored so easily and conveniently in grain elevators. For there, wheat is left exposed at its upper surface to the atmosphere, and during the high humidity that prevails in the warm summer weather, the moisture content of the wheat would increase to a dangerous level were it not that the diffusion takes place so slowly. These results support the conclusions drawn from earlier experiments on the migration of moisture in a mass of wheat under a temperature gradient (1). The experiments also suggest that the time required for moisture to move from the surface of a kernel of wheat into the kernel is, under all ordinary conditions, but a small fraction of the time necessary for the vapor to diffuse up to the surface. In other words, it is the diffusion of water vapor through the air and through overlying layers of grain that limits the amount of moisture taken up by wheat rather than any resistance to moisture movement inherent in the grain itself. Cassie (3) has arrived at a similar conclusion for the change of moisture content of textile fibers. He finds that "the time of diffusion of water vapour from the surface to the interior of the fibre must be of little significance" in comparison with the time of diffusion of the water vapor up to the surface of the fiber. The wheat does, however, possess some quality that resists complete drying.

References

1. ANDERSON, J. A., BABBITT, J. D., and MEREDITH, W. O. S. Can. J. Research, C, 21 : 297-306. 1943.
2. BABBITT, J. D. Nature, 156 : 265. 1945.
3. CASSIE, A. B. D. Repts. Progress Phys. (Phys. Soc. London), 10 : 147. 1944-45.
4. COLEMAN, D. A. and FELLOWS, H. C. Cereal Chem. 2 : 275-289. 1925.
5. DAYNES, H. A. Rubber Chem. and Technol. 12 : 532-534. 1939.
6. GANE, R. J. Soc. Chem. Ind. (London), Trans. 60 : 44-46. 1941.
7. GAY, F. J. J. Council Sci. Ind. Research, 14 : 117-120. 1941.

DRIED WHOLE EGG POWDER

XXVIII. REPRODUCIBILITY AND INTERRELATION OF METHODS OF ASSESSING QUALITY[1]

By Jesse A. Pearce[2] and M. W. Thistle[2]

Abstract

The relation between palatability and fluorescence value, previously established for 33 samples of plain egg powder, was substantiated by comparisons for 118 samples. Fluorescence measurements were more readily reproduced among various laboratories than measurements of potassium chloride value. Batter density measurements were found to be a satisfactory measure of the baking quality of sugar–egg powder and were more convenient than the baking of test cakes. Particle size of spray-dried sugar–egg powder was also related to baking quality; powder falling between 50 and 200 mesh (U.S. Bureau of Standards) yielded the lightest sponge goods.

Introduction

During the course of work reported in earlier papers in this series, several tests of quality in plain dried egg powder were described and some of these have been written into standards governing quality (1, 2, 5). The reproducibility of these tests became the subject of collaborative studies. On sugar–egg powder, measurements of baking volume were inconvenient for control testing and simpler methods were sought. Some of these were also assessed in a collaborative study.

The present paper, describing the results of this work, is divided into two main parts. The first deals with studies on plain egg powder and describes further assessment of the fluorescence–palatability relation (7), and collaborative measurements of fluorescence (8) and potassium chloride values (11). The second deals with studies on sugar–egg powder; it describes the relations between a number of measurements and cake volume (6), and a collaborative study of foam density, batter density (5), and cake volume (5) as methods of assessing baking quality.

Plain Egg Powder

The Palatability–Fluorescence Relation

In the first report (7) on the relation between palatability scores and fluorescence value a correlation coefficient of $-.90^{**}$ was obtained for a 14-man panel testing 33 samples of dried egg. The equation relating these characteristics was

$$y = 2.32 - 0.12\,x,$$

where y is the logarithm of the photofluorometer reading and x is the palatability rating on a scale ranging from 10 for excellent to 0 for inedible samples.

[1] *Manuscript received October 5, 1948.*

Contribution from the Division of Applied Biology, National Research Laboratories, Ottawa. Issued as paper No. 220 of the Canadian Committee on Food Preservation and as N.R.C. No. 1877.

[2] *Biochemist, Food Investigations.*

** *Exceeds the 1% level of statistical significance.*

In the present study, eating-quality assessments by a 12-man panel on 118 samples over a wide range of quality were found to be related to fluorescence values (8) by the equation

$$y = 2.28 - 0.11\,x$$

with a correlation coefficient of $-.84^{**}$. Neither of the parameters of this equation differed significantly from those previously established, and there was no significant difference between the two correlation coefficients.

Collaborative Study of Fluorescence and Potassium Chloride Values

To provide material for this study, a sample of good egg powder was thoroughly mixed, divided into four lots, treated as shown in Table I, canned in 100-gm. samples in No. 1 tins, and held at −40° F. Samples from each

TABLE I

FLUORESCENCE AND POTASSIUM CHLORIDE VALUES ON EGG POWDER OF FOUR QUALITY LEVELS

(Rounded averages of 24 determinations)

Sample designation	Treatment, days at 110° F.	Fluorescence value	Potassium chloride value
Good	None	22	71
	2	29	68
Poor	5	49	43
	9	68	34

treatment were distributed (by air express where necessary) under randomized code numbers, at monthly intervals for four months, to each of the three co-operating laboratories. Each laboratory determined the fluorescence (5) and potassium chloride values (5) on duplicate samples from each tin.

Since duplicate analyses on 'poor' quality powders were significantly more variable than those for 'good' quality powders, the data had to be divided for separate statistical analyses.

The fluorescence measurements made by Laboratory 2 on poor quality egg powders (Table II) were lower than the measurements made in the other two laboratories but, for good egg powders, there was no significant difference attributable to laboratories. The potassium chloride values determined in Laboratory 1, for both good and poor quality powders, were significantly lower than measurements made in either of the other two laboratories. Laboratory 3 consistently recorded high values for the 'good' sample with an average potassium chloride value of 68 (Table I).

An assessment based upon the differences between laboratories, within laboratories, between replicate samples, and between duplicate analyses is given in Table III. The average difference between any two fluorescence

** *Exceeds the 1% level of statistical significance.*

TABLE II

FLUORESCENCE AND POTASSIUM CHLORIDE DETERMINATIONS AT THREE LABORATORIES FOR 'GOOD' AND 'POOR' SAMPLES OF DRIED EGG POWDER

(Averages of 16 determinations)

Laboratories	Fluorescence		Potassium chloride	
	Good samples	Poor samples	Good samples	Poor samples
1	26.5	58.9	67.7	35.3
2	24.8	56.2	69.4	40.6
3	25.0	59.8	70.4	39.6
Necessary difference, 5% level of significance	—	2.7	1.4	2.3

TABLE III

ESTIMATED TOTAL ERRORS OF DETERMINATIONS OF FLUORESCENCE AND POTASSIUM CHLORIDE VALUES

(Based upon results from three laboratories)

Estimates of error	Fluorescence		Potassium chloride	
	Good samples	Poor samples	Good samples	Poor samples
Standard deviation of a single observation	1.6	3.0	2.0	3.5
Average difference between two observations selected at random	1.8	3.4	2.3	4.0
'Maximum' difference between two observations selected at random (5% point)	4.7	9.0	6.1	10.5

value determinations on a good egg powder, under the conditions of this experiment, was likely to be less than 2 units, and the 'maximum' difference (5% point) was likely to be less than 5 units. The corresponding figures for the potassium chloride determination were 2.5 and 6.5 units. Of the two methods of assessing egg powder quality, the fluorescence method was better than the potassium chloride method from the standpoint of reproducibility of results, since, in addition to random errors, determinations of the potassium chloride values were in error because of systematic differences between one laboratory and another.

Sugar–Egg Powder

Since sugar–egg powder is intended for use in baked goods, its baking quality must be controlled. But the baking of test cakes is often inconvenient, and a simpler method of measuring baking quality was desired.

Foaming volume measurements provided useful information in some of the initial experimental work (3), but it was observed that this measure was subject to irregularities (4), and it did not appear to be satisfactory for controlling commercial production.

In the present work, the relations between cake volume and a number of other characteristics were examined, with special attention to determinations of particle size. This was followed by a collaborative test of the cake volume methods in current use. Simple density measurements on cake batter had been suggested as a possible test of baking quality, and density measurements were therefore included in this collaborative study.

Relation Between Some Quality Tests and Cake Volume

The powder used in this part of the study was produced in two Canadian plants using cone-type driers during the fall of 1945: 22 samples were taken at various times from the main drying chamber of one plant and nine samples from the main chamber of the other. The samples were produced under a variety of conditions and represented the range of quality likely to be met in commercial operations.

The analytical measurements made on these powders included determinations of moisture content (11), fluorescence value (8), potassium chloride value (11), pH (5), foaming volume (4, 6, 9), foam stability (6), and cake volume (6). In addition, packing density was determined by measuring the volume occupied by 1 lb. of powder when poured into a container and subjected to three free falls of four inches. Finally, particle size determinations were made by sieving a 1 lb. sample on a Ro-tap shaker for one hour and determining the weight of powder in the various mesh ranges used (U.S. Bureau of Standards). Although this does not provide an exact separation of the powder (10), it was believed satisfactory for the present purpose.

Most of these tests were useless from the standpoint of prediction of cake volume because either the correlation coefficients were too low or different equations had to be used for powders from different plants. Foaming volume was again related to baking volume ($r = .73^{**}$). However, sieve analysis of powders as received from the driers provided the best estimate of cake volume ($R = .80^{**}$), a fact that seemed to warrant further work.

Relation Between Particle Size and Cake Volume

In a preliminary study, an attempt was made to assess the effect of various drying conditions on batches of spray-dried powder of uniform particle sizes, to be obtained by using a fixed nozzle aperture, but this failed because these other drying conditions also had an effect on particle diameter.

During the winter of 1946, cakes were baked using 30 samples of sugar–egg powder from the main drying chambers of eight plants and 14 samples from the secondary collectors of three plants. Samples of the same powders were

** *Exceeds the 1% level of statistical significance.*

sieved as previously described. The prediction equation for powders from the main chambers was:

$$y = 229.3 - 0.094x_1 + 0.556x_2 + 0.450x_3 + 0.453x_4 ,$$

where y is the cake volume in ml. and x_1 , x_2 , x_3 , and x_4 are the percentages of the powder falling between mesh sizes 16 and 50, 50 and 80, 80 and 100, and 100 and 200 respectively. The same equation could be used for powders from the secondary collectors, except that the first term was reduced from 229.3 to 213.3; i.e., on the average, powders from the main chambers gave cakes 16 ml. larger than samples with the same sieve analysis from secondary collectors. However, for both equations, the correlation coefficient was only .75** and the standard error of estimate was ± 11.4 ml. This showed that sieve analysis alone was not a satisfactory measure for controlling the baking quality of commercially produced sugar–egg powders.

These equations indicated that attention should be given to adjusting the conditions of spray-drying to produce powders finer than 50 mesh. Optimum cake volume at 80 to 100 mesh was suggested by an earlier study (6). The poor baking quality of the largest particles may be due to the fact that they dry most slowly and deteriorate while they are wet.

Collaborative Study of Tests of Baking Quality

Since the foregoing work yielded no satisfactory substitute for cake volume measurements, it seemed advisable to examine the baking tests in current use, and coincidentally, to reassess the possibility of using foam density and to assess batter density for predicting baking quality.

For this study, 30 samples of spray-dried sugar–egg were drawn from Canadian commercial production during the summer of 1946: 20 samples were obtained from main drying chambers and 10 samples from secondary collectors. Each sample was thoroughly mixed in a mechanical device and aliquots were packed in No. 1 tins and sent to the participating laboratories for triplicate analyses. The procedure described elsewhere (5) for determining batter density and cake volume was used with minor modifications* by most of the laboratories. Laboratory 1 used a simpler procedure (6). Laboratory 5 used both procedures and their results for the simpler procedure are listed as Laboratory 5*A*. Foam density was determined on the batter before the addition of flour.

For powders from the main drying chambers, differences between samples were nearly all within the limits of experimental error and hence failed to provide any information on the interrelations under study. For secondary collector powders, the correlation coefficients were considerably higher and most of them were statistically significant (Tables IV and V).

* *The details, if desired, can be obtained by requesting a copy of Interim Report No. 46-12-1, Division of Applied Biology, National Research Laboratories, Sussex St., Ottawa.*

** *Exceeds the 1% level of statistical significance.*

TABLE IV

INTERRELATION BETWEEN THE METHODS USED BY FIVE LABORATORIES FOR ASSESSING THE BAKING QUALITY OF 10 SAMPLES (SECONDARY COLLECTOR) OF SUGAR–EGG POWDER

(Simple correlation coefficients between laboratories)

Methods	Lab. No. 2	Lab. No. 3	Lab. No. 4	Lab. No. 5	Lab. No. 5A
CAKE VOLUME					
Lab. No. 1	.81**	.92**	.88**	.82**	.71*
Lab. No. 2		.75*	.60	.59	.52
Lab. No. 3			.78**	.66*	.74*
Lab. No. 4				.89**	.75*
Lab. No. 5					.85**
FOAM DENSITY					
Lab. No. 1	.52	.87**	.75*	.79**	
Lab. No. 2		.51	.50	.63	
Lab. No. 3			.86**	.80**	
Lab. No. 4				.64*	
BATTER DENSITY					
Lab. No. 1	.59	.86**	.67*	.93**	
Lab. No. 2		.55	.61	.70*	
Lab. No. 3			.75*	.92**	
Lab. No. 4				.74*	

* *Attains 5% level of statistical significance.*
** *Attains 1% level of statistical significance.*

TABLE V

INTERRELATION BETWEEN THE METHODS USED FOR ASSESSING THE BAKING QUALITY OF 10 SAMPLES (SECONDARY COLLECTOR) OF SUGAR–EGG POWDER, AT EACH OF FIVE LABORATORIES

(Simple correlation coefficients between methods)

Laboratories	Cake volume × foam density	Foam density × batter density	Cake volume × batter density
1	−.88**	.99**	−.87**
2	−.61	.84**	−.87**
3	−.84**	.99**	−.85**
4	−.66*	.83**	−.79**
5	−.95**	.86**	−.88**
5A	−.79**	.86**	−.87**

* *Attains 5% point of statistical significance.*
** *Attains 1% point of statistical significance.*

Table V shows the interrelation, within laboratories, between the various methods of measuring baking quality. At some laboratories, correlation coefficients between cake volume and foam density were too low for prediction purposes. The relation between foam density and batter density is of little practical importance. However, the highly significant correlation coefficients for the relation between cake volume and batter density indicated that a batter density test might be useful for measuring baking quality. Calculations

showed that sugar–egg powder giving a batter with density greater than 0.43 by any of the procedures used was unsuitable for use in the best class of sponge goods. Therefore, during the past two years, a batter density test (5) has been used to control the baking quality of sugar–egg powder exported from Canada.

Acknowledgments

The laboratories of the following institutions collaborated with the National Research Laboratories, Ottawa, throughout this work: Borden's, New York; Canada Egg Products Limited, Saskatoon; Science Service and Experimental Farms Service of the Dominion Department of Agriculture, Ottawa; and Swift and Company, Chicago. Without their wholehearted co-operation these studies would not have been possible. We are particularly indebted to Dr. L. Mink of Swift and Company, Chicago, who made the original suggestion that measurements of batter density might be useful in predicting the baking quality of sugar–egg powder.

References

1. CANADA, DEPARTMENT OF AGRICULTURE. Special Products Board Requirement No. 6. Feb. 28, 1944.
2. CANADA, DEPARTMENT OF AGRICULTURE. Special Products Board Requirement No. 7. June 6, 1947.
3. HAY, R. L. and PEARCE, J. A. Can. J. Research, F, 24 : 168-182. 1946.
4. HAY, R. L. and PEARCE, J. A. Can. J. Research, F, 24 : 430-436. 1946.
5. NATIONAL RESEARCH COUNCIL AND SCIENCE SERVICE OF THE DEPARTMENT OF AGRICULTURE, CANADA. The official methods used for assessing quality in Canadian sugar dried whole egg powders. Ottawa. June 6, 1947.
6. PEARCE, J. A., BROOKS, J., and TESSIER, H. Can. J. Research, F, 24 : 420-429. 1946.
7. PEARCE, J. A. and THISTLE, M. W. Can. J. Research, D, 20 : 276-282. 1942.
8. PEARCE, J. A., THISTLE, M. W., and REID, M. Can. J. Research, D, 21 : 341-347. 1943.
9. REID, M. and PEARCE, J. A. Can. J. Research, F, 23 : 239-242. 1945.
10. TESSIER, H., MARIER, J. R., and PEARCE, J. A. Can. J. Research, F, 25 : 149-159. 1947.
11. THISTLE, M. W., PEARCE, J. A., and GIBBONS, N. E. Can. J. Research, D, 21 : 1-7. 1943.

A NICKEL–ALUMINUM–MOLYBDENUM CREEP RESISTANT ALLOY[1]

By H. V. Kinsey[2] and M. T. Stewart[3]

Abstract

This paper describes a preliminary study of alloys of nickel and aluminum modified with molybdenum. The purpose of this work is to develop an alloy for use under conditions of stress at temperatures of 815° C. (1500° F.) and over. The room temperature mechanical properties of alloys of nickel and aluminum, and the influence of molybdenum on these properties, have been investigated. Certain combinations of nickel, aluminum, and molybdenum have been shown to possess tensile strengths well over 100,000 lb. per sq. in. at room temperature, and it has been demonstrated that certain characteristic microstructures, dependent upon the ratio of nickel to aluminum, are essential for the realization of these high strengths. Creep-rupture tests at 815° C. (1500° F.) have been carried out on typical nickel–aluminum–molybdenum alloys. The results have shown that certain of these alloys are superior in many respects to existing high temperature alloys, when tested under creep-rupture conditions at 815° C. (1500° F.). The same characteristics of microstructure that are essential for high room temperature strengths were also found to be necessary to obtain good creep-rupture characteristics at 815° C. (1500° F.).

Introduction

So much has been written on the subject of alloys for use in gas turbine blades that the more important requirements for such materials are now widely recognized. They must have chemical stability to ensure resistance to corrosion by hot combustion gases. A second requirement is stability of microstructure at anticipated operating temperatures, to minimize the deterioration of mechanical properties during long exposure to elevated temperatures. Also, a high strength–weight ratio is desirable in alloys under consideration for gas turbine blades, since the stress causing creep in these parts is generated by centrifugal force.

The high melting points and relatively low densities of the nickel-rich nickel–aluminum alloys, specifically of the intermetallic compound NiAl, suggested that an investigation of the creep properties of alloys based on the nickel–aluminum system might be worth while. The nickel–aluminum phase diagram (1) is presented in Figs. 1 and 2.

All the alloys to be dealt with in this paper were melted by high frequency induction in magnesia crucibles. Test bars were centrifugally cast into molds produced by the "lost wax" precision casting technique.

All room temperature tensile tests were made on the Hounsfield tensometer, using the test-bar design shown in Fig. 3. All creep and stress-rupture tests

[1] *Manuscript received September 22, 1948.*

Published by permission of the Director, Mines, Forests and Scientific Services Branch, Department of Mines and Resources, Ottawa, Canada.

[2] *Metallurgical Engineer; Head, High Temperature Metals Laboratory, Physical Metallurgy Research Laboratories, Division of Mineral Dressing and Metallurgy, Bureau of Mines, Ottawa.*

[3] *Junior Research Officer, Associate Committee on High Temperature Metals, National Research Council of Canada, Ottawa, Canada.*

were obtained with the test bar design shown in Fig. 4. Note that one end of this bar is hollow, to promote directional solidification.

The metal temperatures of the melts cast into the large test bars (see Fig. 4) were measured with an immersion platinum–rhodium thermocouple used in conjunction with a high speed potentiometer-type temperature recorder.

The metals used in this work are listed in Table I, together with the analyses obtained from the suppliers.

TABLE I

COMPOSITIONS OF MATERIALS USED

Material	Chemical analysis, %
Nickel (electrolytic)	Ni, 99.9
Cobalt (electrolytic)	Co, 99.5. Major impurity: Cu.
Aluminum	Al, 99.5. Impurities: Fe, Mn, Si.
Molybdenum	Mo, 99.5. Impurities: Mn, Si, Fe.

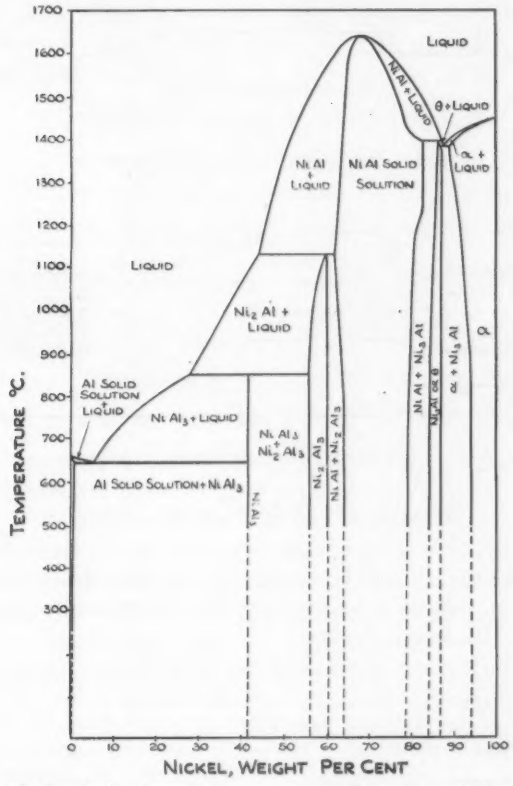

FIG. 1. *Nickel–aluminum phase diagram over complete range. (After Alexander and Vaughan (1).)*

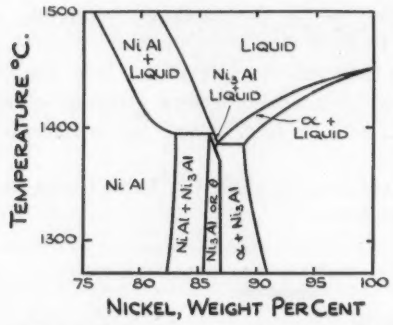

FIG. 2. *Nickel–aluminum phase diagram for the range of 75 to 100% nickel. (After Alexander and Vaughan (1).)*

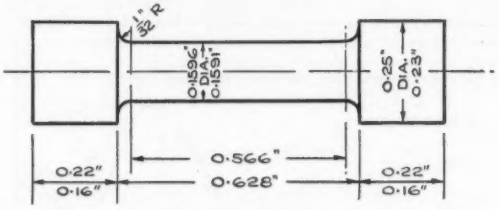

FIG. 3. *Tensile bar for Hounsfield tensometer.*

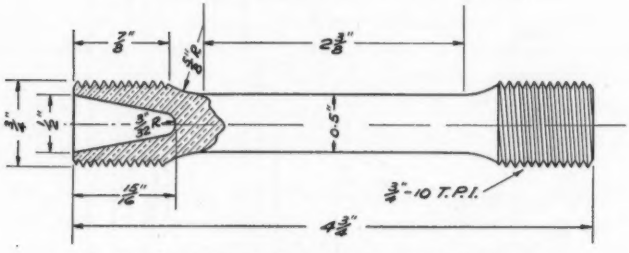

FIG. 4. *Precision cast ¼ in. diameter creep test bar.*

System of Alloy Nomenclature

With the exception of the preliminary group of four binary alloys of nickel and aluminum, all the alloys to be discussed were made up of nickel, aluminum, and molybdenum. In order to facilitate the discussion of these alloys, the following nomenclature was devised.

If the Ni : Al ratio and the amount of molybdenum present are stated, then the alloy is fully described. For example, let the Ni : Al ratio be 10.3 : 1 and the amount of molybdenum present be 14.7%. Then the alloy is identified by the expression 103M147. The letter "M" is included to indicate that the third element present is molybdenum. If the Ni : Al ratio is 7.6 : 1 and the molybdenum content is 8.2%, then the expression 76M82 identifies the alloy.

Nickel–Aluminum Alloys

Table II lists the phase zone boundary limits in the nickel-rich portion of the nickel–aluminum phase diagram (see Figs. 1 and 2). These boundary limits are stated in terms of the ratio of nickel to aluminum.

TABLE II

PHASE ZONE BOUNDARY LIMITS BELOW 950° C. (1742° F.) IN THE NICKEL–ALUMINUM SYSTEM

Ni : Al ratio	Phases present
2.3 : 1 to 3.76 : 1	NiAl solid solution
3.76 : 1 to 5.25 : 1	NiAl + Ni_3Al
5.25 : 1 to 6.7 : 1	Ni_3Al
6.7 : 1 to 15.6 : 1	Ni_3Al + alpha solid solution
Over 15.6 : 1	Alpha solid solution

Four binary alloys of nickel and aluminum, characteristic of the first four phase zones listed in Table II, were chosen as a starting point for this work. These alloys are listed in Table III.

TABLE III

BINARY NICKEL–ALUMINUM ALLOYS

Alloy No.	Chemical analysis, %		Ni : Al ratio		Anticipated phases
	Nickel	Aluminum	Sought	Obtained	
1	73.08	26.92	3 : 1	2.7 : 1	NiAl
2	83.19	16.81	4 : 1	4.9 : 1	NiAl + Ni_3Al
3	84.70	15.30	5.6 : 1	5.6 : 1	Ni_3Al
4	92.2	7.8	9 : 1	11.8 : 1	Ni_3Al + alpha solid solution

Hounsfield tensometer test bars were cast and the room temperature mechanical properties given in Table IV were determined.

TABLE IV

ROOM TEMPERATURE MECHANICAL PROPERTIES OF NICKEL–ALUMINUM ALLOYS

Alloy No.	Tensile strength, p.s.i.		Average elongation, %	Vickers hardness value (30 kgm. load)
	Average	Maximum		
1	Nil	Nil	Nil	389
2	28,500	30,000	"	404
3	60,000	62,000	"	265
4	64,667	77,000	18.3	346

The properties listed in Table IV are shown plotted against the Ni : Al ratio in Fig. 5. It will be noted that Alloys 3 and 4 above, which on the basis of their Ni : Al ratio would not be expected to show any of the NiAl constituent, possess the most promising room temperature mechanical properties.

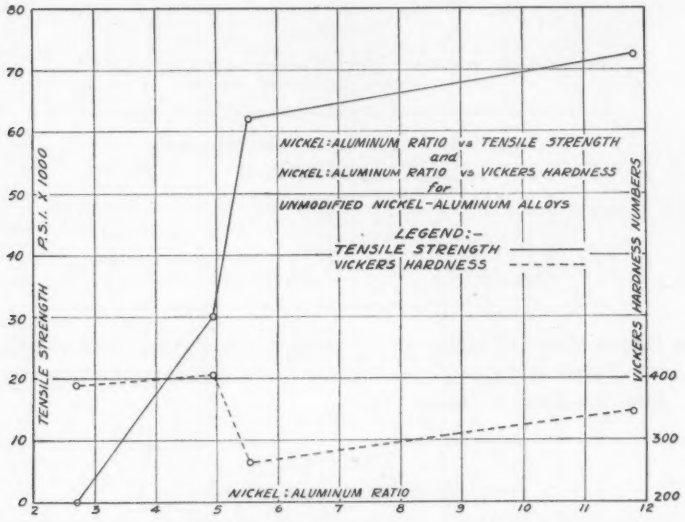

FIG. 5. *Mechanical properties vs. Ni : Al ratio.*

Metallography of Nickel–Aluminum Alloys

Figs. 6 to 11, inclusive, are photomicrographs showing the microstructure of Alloys 1, 2, 3, and 4, respectively. Alloy 1, with a Ni : Al ratio of 2.7 : 1, has only one phase, as would be expected. Alloys 2 and 3 have two phases. Alloy 2 has a Ni : Al ratio of 4.9 : 1, which indicates the presence of both NiAl and Ni_3Al. Alloy 3 has a Ni : Al ratio of 5.6 : 1. Under equilibrium conditions this alloy should consist structurally of a single phase, Ni_3Al. However, since all the microstructures under consideration are of "as cast" alloys, the presence of two phases in Alloy 3 is not surprising. These two phases would be expected to be NiAl and Ni_3Al.

FIG. 6. *Alloy No. 1, as cast. Electrolytic polish, Vilella's etchant. ×200. Ni, 73.08%; Al, 26.92%.*

FIG. 7. *Alloy No. 2, as cast. Mechanical polish, Vilella's etchant. ×200. Ni, 83.19%; Al, 16.81%.*

FIG. 8. *Alloy No. 3, as cast. Mechanical polish, Vilella's etchant. ×200. Ni, 84.70%; Al, 15.30%.*

FIG. 9. *Same as Fig. 8. ×750.*

FIG. 10. *Alloy No. 4, as cast. Mechanical polish; etchant, ferric chloride plus hydrochloric acid in alcohol. ×200. Ni, 92.2%; Al, 7.8%.*

FIG. 11. *Same as Fig. 10. ×750.*

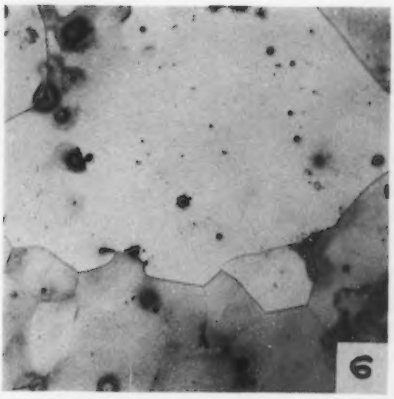
6


7

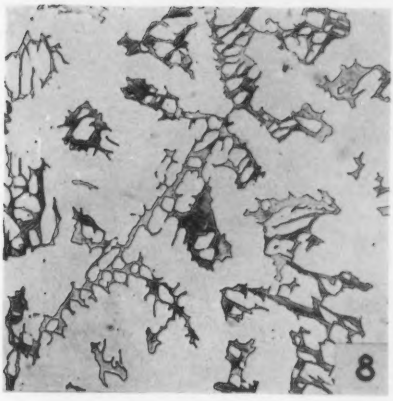
8

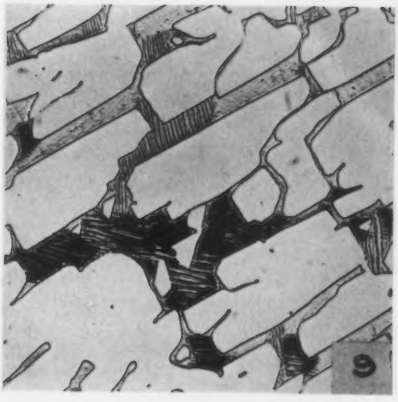
9

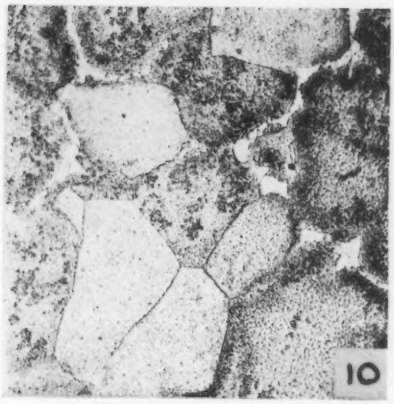
10

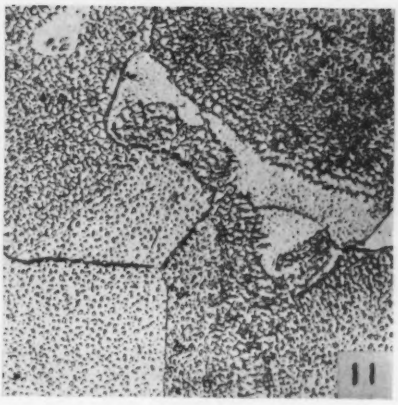
11

A comparison of the microstructures of Alloys 2 and 3, as shown in Figs. 7 and 8, will enable us to establish the identity of these two phases. There is a dark-etching phase and a light-etching phase present. Alloy 2, which has a lower Ni : Al ratio than Alloy 3, should be expected to have more of the NiAl phase than Alloy 3. Since there is more of the dark-etching phase in Alloy 2 than in Alloy 3, it is assumed that this dark-etching phase in these structures is NiAl and the light-etching phase is Ni_3Al.

The Ni : Al ratio of Alloy 4 indicates that it will consist structurally of two phases, alpha and Ni_3Al. Its microstructure, as shown in Figs. 10 and 11, indicates the presence of two phases. Most of the structure is characteristic of the structure obtained when a secondary phase precipitates from a primary solid solution owing to a shift in solubility with falling temperature. From the position of this alloy in the nickel–aluminum system, it would be expected to freeze out largely as alpha solid solution and to precipitate Ni_3Al on cooling below 1200° C. It is apparent, then, that the precipitated phase in this alloy is Ni_3Al and that the matrix is alpha solid solution.

Attention is drawn to the clear white areas visible in Fig. 10. According to Alexander and Vaughan (1), these are areas of Ni_3Al that, on freezing, were the alpha-Ni_3Al eutectic. They have shown that this eutectic cannot exist below 1370° C., owing to the increase of solubility of nickel in Ni_3Al that occurs between 1385° C. and 1370° C., which results in the disappearance of what little alpha has separated in the eutectic. The fact that some eutectic formed in Alloy 4 may be explained by the fact that sufficient segregation occurred during freezing to permit this formation.

Nickel-Aluminum-Molybdenum Alloys

The fact that molybdenum is a vital constituent of many high temperature alloys prompted a decision to investigate its influence on nickel–aluminum alloys. The program adopted involved preliminary tests at room temperature, to be followed by creep and creep rupture tests on such alloys as proved castable and displayed promise from consideration of their room temperature properties.

For a preliminary study of room temperature properties, these molybdenum-modified alloys were divided into four groups, each group having a constant Ni : Al ratio, so that, in effect, an attempt was made to study the influence of various molybdenum additions to the alloys listed in Table III. Alloys 1, 3, and 4 of Table III were the starting point for three of these groups. The fourth group was based on a Ni : Al ratio of 19 : 1, which represents a single-phase alpha solid solution alloy.

These alloys are listed in Table V. Fig. 12 shows the position of these alloys on the ternary nickel–aluminum–molybdenum triangle. This chart also contains the nickel–aluminum phase diagram (1) and the nickel–molybdenum phase diagram (2).

TABLE V

CHEMICAL ANALYSES OF NICKEL–ALUMINUM–MOLYBDENUM ALLOYS OBTAINED

Alloy sought	Alloy obtained	Chemical analysis, %		
		Nickel	Aluminum	Molybdenum
30M44	30M47	71.24	23.73	4.72
30M162	30M149	63.80	21.24	14.91
30M250	35M202	61.90	17.90	20.2
30M350	30M247	56.65	18.70	24.65
30M450	29M386	45.55	15.83	38.62
30M550	28M511	35.95	12.95	51.10
57M50	54M39	81.02	15.04	3.94
57M100	57M106	76.04	13.36	10.60
57M150	55M156	71.36	13.07	15.57
57M250	57M131	74.0	12.9	13.10
57M350	59M320	58.2	9.8	32.0
57M450	57M384	52.4	9.2	38.4
57M550	56M443	47.3	8.4	44.3
90M50	90M53	85.25	9.48	5.27
90M100	86M104	80.2	9.37	10.43
90M150	130M177	76.5	5.83	17.67
90M250	94M248	68.0	7.20	24.80
90M350	89M357	57.8	6.5	35.7
190M50	177M46	90.5	4.95	4.55
190M100	165M105	84.4	5.10	10.50
190M150	172M161	79.3	4.6	16.1
190M250	185M255	70.7	3.8	25.5

Room Temperature Mechanical Properties of Nickel–Aluminum–Molybdenum Alloys

Three bars from each of the alloy heats listed in Table V were pulled in room temperature tensile tests. The results are listed in Table VI. Vickers hardness values are also recorded in this table.

The results of these tensile tests are summarized graphically in Fig. 13, which shows the influence of molybdenum on the tensile strength and hardness of alloys of several nickel–aluminum ratios. Evidently molybdenum is most effective as a strengthener when nickel and aluminum are in such a ratio that a binary alloy of nickel and aluminum would consist structurally of Ni_3Al + alpha solid solution, or alpha solid solution alone (see Fig. 1).

Metallography of Nickel–Aluminum–Molybdenum Alloys

Figs. 14 to 21 illustrate the significant metallographic features of the alloys having the chemical and mechanical properties listed in Tables V and VI respectively.

These photomicrographs should be interpreted with reference to the phase zone boundary limits set out in Table II.

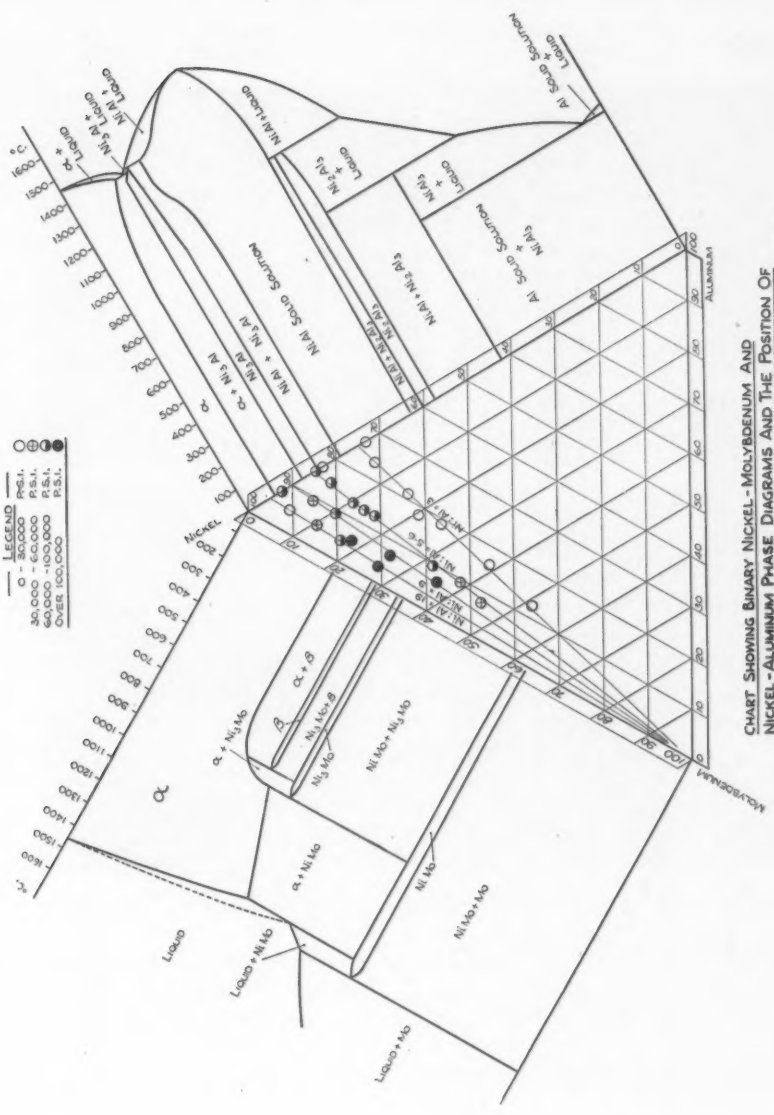

CHART SHOWING BINARY NICKEL-MOLYBDENUM AND NICKEL-ALUMINUM PHASE DIAGRAMS AND THE POSITION OF THE ALLOYS MADE IN THE NICKEL-ALUMINUM-MOLYBDENUM SYSTEM

FIG. 12.

TABLE VI

ROOM TEMPERATURE MECHANICAL PROPERTIES FOR NICKEL–ALUMINUM–MOLYBDENUM ALLOYS

Alloy	Tensile strength, p.s.i.		Average elongation, %	Vickers hardness value (30 kgm. load)
	Average	Maximum		
30M47	4,000	4,000	Nil	473
30M149	5,500	7,000	"	488
35M202	14,500	15,000	"	412
30M247	17,700	22,000	"	422
29M386	18,667	25,000	"	453
28M511	21,000	23,000	"	481
54M39	64,000	65,000	"	305
57M106	81,000	90,000	"	411
55M156	68,500	70,000	"	377
57M131	73,667	82,000	"	387
59M320	62,000	64,000	"	390
57M384	44,333	59,000	"	400
56M443	42,667	49,000	"	402
90M53	51,000	57,000	"	215
86M104	80,000	83,000	7.0	253
130M177	132,333	140,000	10.7	437
94M248	131,000	136,000	Nil	406
89M357	105,000	107,000	"	413
177M46	16,000	17,000	"	94.1
165M105	35,000	37,000	"	231
172M161	71,000	77,000	16.0	236
185M255	130,000	130,000	5.5	391

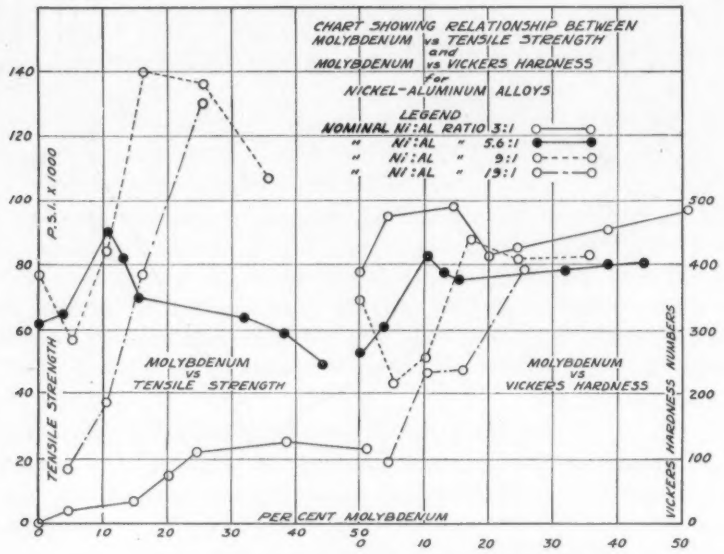

FIG. 13. *Mechanical properties of Ni-Al-Mo alloys.*

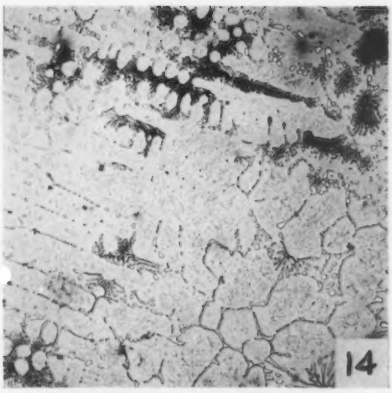

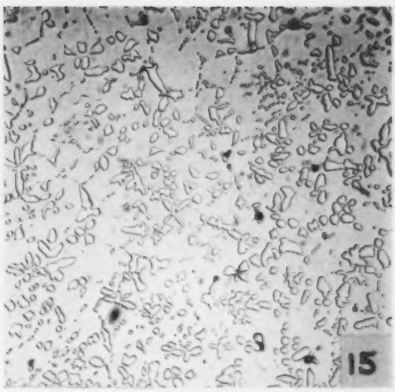

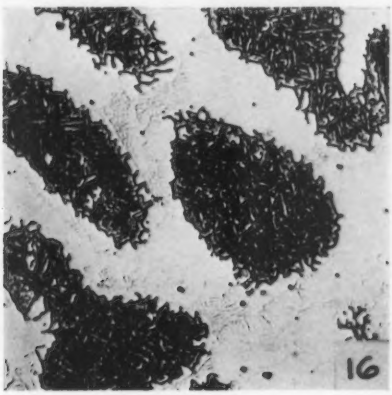

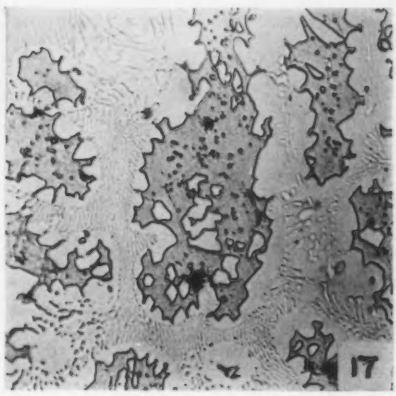

FIG. 14. *Alloy 30M149, as cast. Mechanical polish, Vilella's etchant. ×200. Ni, 63.8%; Al, 21.24%; Mo, 14.91%.*

FIG. 15. *Alloy 30M247, as cast. Mechanical polish, Vilella's etchant. ×200, Ni, 56.65%; Al, 18.70%; Mo, 24.65%.*

FIG. 16. *Alloy 57M106, as cast. Mechanical polish, Vilella's etchant. ×750. Ni, 76.04%; Al, 13.36%; Mo, 10.60%.*

FIG. 17. *Alloy 55M156, as cast. Mechanical polish, Vilella's etchant. ×750. Ni, 71.36%; Al, 13.07%; Mo, 15.57%.*

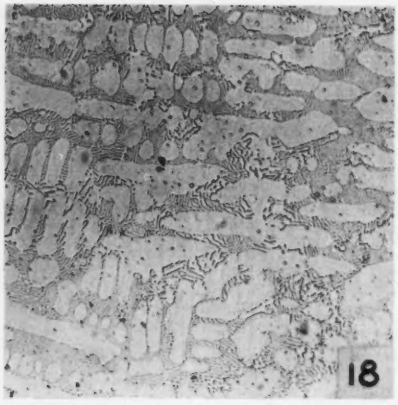

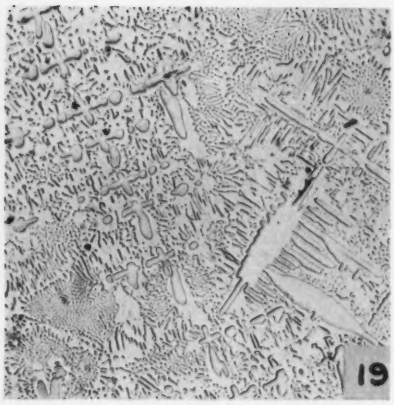

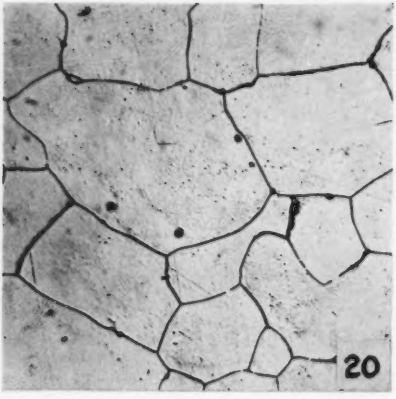

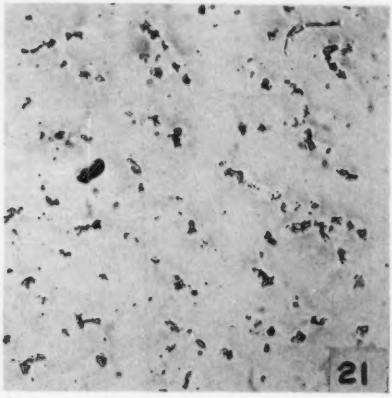

FIG. 18. *Alloy 94M248, as cast. Mechanical polish, Vilella's etchant. ×200. Ni, 68%; Al, 7.20%; Mo, 24.8%.*

FIG. 19. *Alloy 89M357, as cast. Mechanical polish, Vilella's etchant. ×200. Ni, 57.8%; Al, 6.5% Mo, 35.7%.*

FIG. 20. *Alloy 165M105, as cast. Mechanical polish; etchant, ferric chloride plus hydrochloric acid in alcohol. ×200. Ni, 84.4%; Al, 5.1%; Mo, 10.5%.*

FIG. 21. *Alloy 185M255, as cast. Mechanical polish; etchant, ferric chloride plus hydrochloric acid in alcohol. ×200. Ni, 70.7%; Al, 3.8%; Mo, 25.5%.*

When the Ni : Al ratio is 3 : 1, the alloy may be expected to be basically NiAl. The addition of molybdenum to such an alloy causes the formation of a second phase. This is shown in Figs. 14 and 15, which are the microstructures of Alloys 30M149 and 30M247 respectively.

In as-cast binary nickel–aluminum alloys with a Ni : Al ratio of 5.7 : 1, previous work has shown that two phases, namely NiAl and Ni_3Al, may be present. These phases have been tentatively identified in Figs. 7 and 8. Based on this identification, it may be assumed that the dark-etching phase in the nickel–aluminum-molybdenum alloys having a Ni : Al ratio of 5.7 : 1 will be NiAl. The structures of typical alloys of this group, Alloys 57M106 and 55M156, are shown in Figs. 16 and 17.

The eutectic appearing in Alloys 57M106 and 55M156 is characteristic of the presence of molybdenum. This eutectic can be caused to disappear from Alloy 57M106 by heating to 1000° C. (1832° F.). It is therefore assumed that the presence of this eutectic in Alloy 57M106 in the as-cast condition is due to segregation on freezing, and that under conditions approaching equilibrium it will not occur in this alloy.

In alloys of the 9 : 1 Ni : Al ratio group, molybdenum again causes the occurrence of a characteristic phase. This is illustrated by Fig. 18, which is the microstructure of Alloy 94M248. (The NiAl phase is absent from this group of alloys.) As the molybdenum content increases, this phase becomes more massive, as is shown by Fig. 19, which is the microstructure of Alloy 89M357.

Alloys having a Ni : Al ratio greater than 15 : 1 are structurally single-phase alpha solid solution up to at least 16% Mo; Fig. 20 is characteristic of this microstructure. At 25% Mo a second phase appears; this may be seen in Fig. 21.

An attempt has been made tentatively to establish the identity of the phase that is associated with the presence of molybdenum. This identification is based on the work of Ellinger (2).

It would appear that this phase, which occurs as a eutectic in Alloys 57M106, 55M156, 94M248, and 89M357 (Figs. 16, 17, 18, and 19), and in a primary form in Alloys 30M149, 30M247 and 89M357 (Figs. 14, 15, and 20), could be the delta (NiMo) phase of the nickel–molybdenum system.

On this basis, Alloys 30M149, 30M247, and 89M357 are all hypereutectic with respect to molybdenum, since primary NiMo is present. The absence of primary NiMo in Alloys 57M106, 55M156, and 94M248 would indicate that these alloys are hypoeutectic with respect to molybdenum.

Summary of Metallographic Features

1. The addition of molybdenum to alloys of nickel and aluminum causes the appearance of a characteristic phase tentatively identified as NiMo. This phase will occur in the primary form when the alloy is hypereutectic with respect to molybdenum and it will occur in the eutectic form when the alloy is hypoeutectic with respect to molybdenum.

2. The limiting molybdenum content at which the phase NiMo will occur varies with the nickel : aluminum ratio.

3. The NiAl phase persists in the ternary alloys of nickel, aluminum, and molybdenum at nickel : aluminum ratios generally similar to those in the binary nickel–aluminum alloys.

4. The presence of the NiAl phase has a marked weakening effect on the alloy and renders it less responsive to strengthening by additions of molybdenum.

Creep-rupture Properties of Some Nickel–Aluminum–Molybdenum Alloys at 815° C. (1500° F.)

The alloys selected for creep-rupture tests are listed in Table VII. This choice was dictated by the wish to include a representative alloy of each of the groups shown in Table V. The molybdenum contents were chosen from consideration of the room temperature properties presented in Table VI. The cast test bars were of the design shown in Fig. 4.

TABLE VII

ALLOYS SELECTED FOR CREEP-RUPTURE STUDIES

Alloy	Chemical analysis, %		
	Nickel	Aluminum	Molybdenum
30M250	56	19	25
56M100	76	15	10
90M150	76	9	15
90M200	72	8	20
190M250	71	4	25

The liquidus and solidus temperatures of these alloys were first measured as an aid in determining the proper casting temperature. Both the freezing curve technique, employing an immersion platinum–rhodium thermocouple, and the metallographic method were employed. Table VIII lists the results of these measurements.

TABLE VIII

LIQUIDUS AND SOLIDUS TEMPERATURES

Alloy	Chemical analysis, %			Freezing curve data		Metallographic data
	Ni	Al	Mo	Liquidus, °C.	Solidus, °C.	Solidus, °C.
35M246	58.6	16.6	24.6	1625	1540	Not determined
76M151	75.6	16.9	15.1	1415	1290	" "
95M138	79.0	8.3	13.8	1370	1360	1325 – 1340
106M217	72.9	6.9	21.7	1360	1290	1285 – 1300
213M257	72.4	3.4	25.7	1375	1270	Not determined

On the basis of the data listed in Table VIII, a casting temperature of 1650° C. (3002° F.) was chosen for all alloys but 30M250, for which a casting temperature of 1750° C. (3182° F.) was used. The temperature of the test-bar molds was held within the range of 649° to 677° C. (1200° to 1250° F.).

All test bars cast were subjected to X-ray inspection as a final check on soundness. It was not possible to produce good test bars from Alloy 30M250. Two heats were attempted. All bars of Alloy 30M250 produced contained shrinks and hot tears. This alloy was therefore eliminated at this point.

The chemical analysis of the alloy heats that produced good test bars are listed in Table IX.

TABLE IX

CHEMICAL ANALYSIS OF ALLOYS PRODUCING RADIOGRAPHICALLY SOUND TEST BARS

Alloy	Chemical analysis, %				
	Ni	Al	Mo	Fe	Si
53M104	74.9	14.2	10.4	0.1	0.37
90M158	75.6	8.4	15.8	0.4	0.24
95M255	66.5	7.0	25.5	0.8	0.16
258M252	72.4	2.8	25.2	0.06	0.25

All but two of the creep-rupture tests were carried out at 815° C. (1500° F.). The results of these tests are summarized in Table X. The elongation vs. time curves for Alloys 90M158 and 95M255 are presented in Figs. 22 and 23.

TABLE X

SUMMARY OF CREEP-RUPTURE TESTS AT 815° C. (1500° F.)

Alloy	Stress, p.s.i.	Elongation on application of load, %	Hours to rupture	Total elongation, %	Minimum creep rate, % per hr.	Remarks
53M104	29,948	0.82	1	11		
	20,030	0.31	6	12½		
90M158	35,000	—	112	0.5	—	Extensometers not functioning
	29,945	0.15	285	2	0.0018	
	27,440	0.11	664	2.5	0.0015	
95M255	40,000	0.278	100	4.5	0.033	
	35,000	—	352	6	—	Extensometers not functioning
	35,000	0.25	236	6	0.012	See note below*
	30,000	0.18	556	4	0.0027	
	27,600	0.21	913	3	0.0022	
258M252	25,000	0.15	75	—	—	
	22,500	0.12	117	1.5	—	
	13,500	—	442	—	—	Extensometers not functioning
95M255	15,000	Test temperature, 982° C. (1800° F.). Adapter bar broke in seven hours. Elong. 1¼%*				

* NOTE: *After being stressed to 15,000 p.s.i. at 982° C. for seven hours, this bar was used for a test at 815° C. with a stress of 35,000 p.s.i. Between these tests the bar was unstressed and cooled to room temperature.*

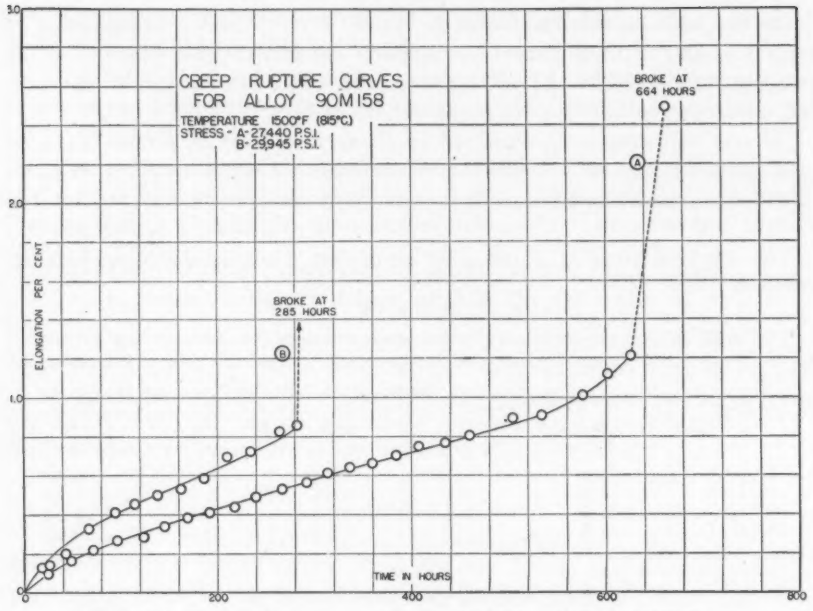

FIG. 22. *Creep-rupture curves, Alloy No. 90M158 at 815° C. (1500° F.).*

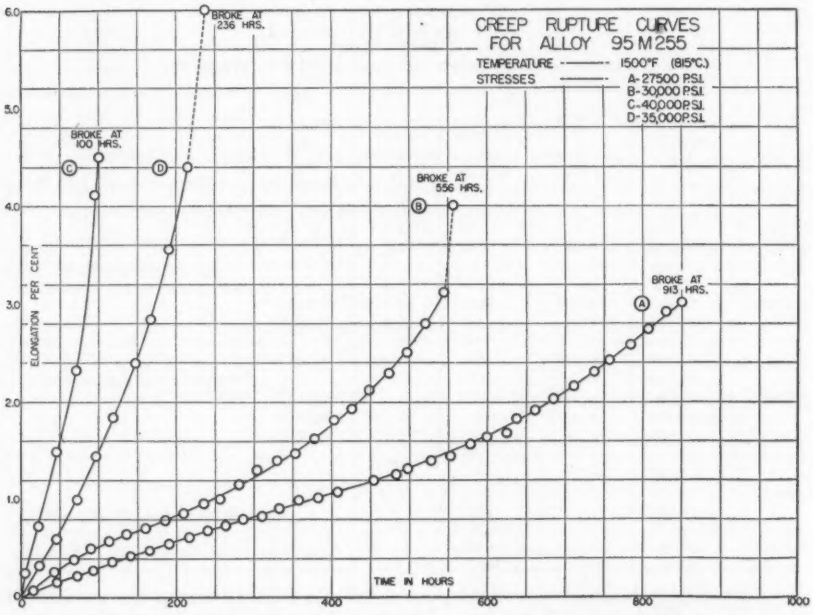

FIG. 23. *Creep-rupture curves, Alloy No. 95M255 at 815° C. (1500° F.).*

In certain tests, as noted in Table X, the extensometers were not functioning properly, and therefore no creep data are available from these tests.

It will be noted that one test is reported on Alloy 95M255 at 982° C. (1800° F.), using a stress of 15,000 p.s.i. This test lasted for seven hours before the adapter bar broke, at which time the test bar had elongated 1½%. This test bar was later put into test at 815° C. (1500° F.) under a stress of 35,000 p.s.i. It lasted for 236 hr. as compared to the 352 hr. of a duplicate bar that had been tested in the as-cast condition at 815° C. (1500° F.) using a stress of 35,000 p.s.i. All creep data for 35,000 p.s.i. at 815° C. (1500° F.) for Alloy 95M255 were obtained from the bar that was first tested at 982° C. (1800° F.) and subsequently tested at 815° C. (1500° F.).

The graphs shown in Figs. 24 and 25 summarize the results of the creep-rupture tests on Alloys 90M158 and 95M255 and compare these alloys with some of the existing standard and improved high temperature alloys. The chemical analyses of the alloys used for comparison purposes are listed in Table XI. These alloys are: a standard vitallium alloy, 30V-2(4); two modified vitallium alloys, 73J(4), and X-63(3); and alloys S-816 and Inconel "X".

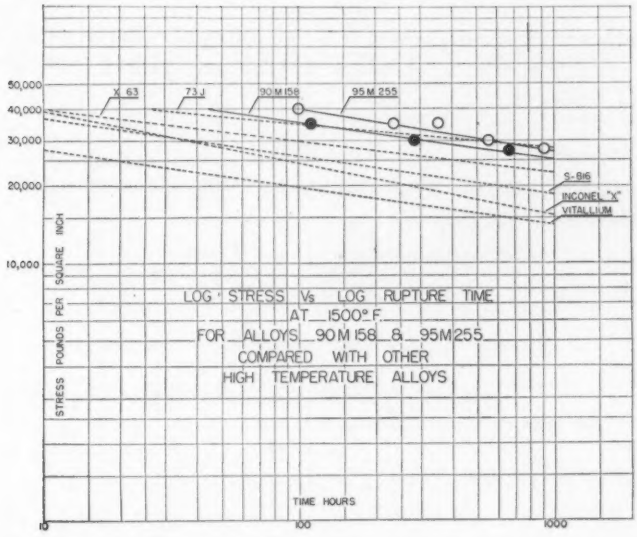

FIG. 24. *Graphical summary of creep-rupture tests at 815° C. (1500° F.) on alloys 90M158 and 95M255, and comparison with other high temperature alloys.*

Fig. 24 is a graph of log stress vs. log rupture time. Fig. 25 contains two graphs, one showing log stress vs. log time to 0.5% total creep strain, and the other showing log stress vs. log minimum creep rate.

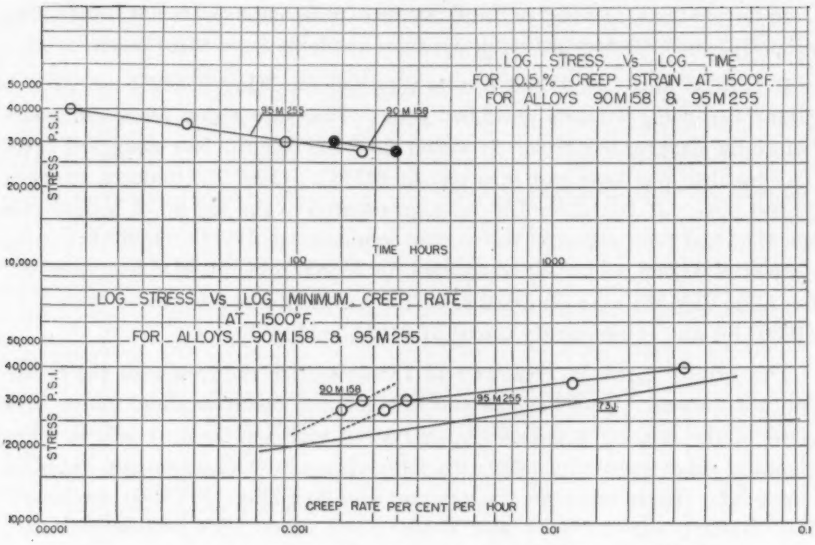

FIG. 25. *Creep-rupture results and comparisons at 815° C. (1500° F.).*

As a further basis of comparison, it is interesting to consider specific gravity values of existing alloys and of Alloys 90M158 and 95M255. These data are included in Table XI.

TABLE XI

CHEMICAL ANALYSES AND SPECIFIC GRAVITY OF COMPARATIVE ALLOYS

Element	Cast vitallium type			Wrought		90M158	95M255
	73J	X-63	30V-2	S-816	Inconel "X"		
	%						
Cobalt	60	57.5	69	43			
Nickel	6	10		20	73	75.6	66.5
Chromium	23	25	23	20	15		
Molybdenum	6	6	6	4		15.8	25.5
Tantalum	2						
Columbium				3.5	1		
Tungsten				4.5			
Titanium					2.5		
Aluminum					0.7	8.4	7.0
Iron				4 max.	7	0.4	0.8
Manganese		0.5		1.5	0.5		
Silicon		0.5		0.5	0.4	0.24	0.16
Carbon	0.75	0.5	0.3	0.35	0.04		
Specific gravity	*	*	8.30	8.66	8.3	7.6	8.0

* *Not available.*

The data presented in Table XII indicate for the various alloys the stress to cause both rupture and 0.5% total creep strain in 100, 1000, and 5000 hr. In Table XIII the data are arranged on a basis of minimum creep rate.

TABLE XII

CREEP-RUPTURE DATA AT 815° C. (1500° F.), SUMMARIZED ON A TIME BASIS

Alloy	100 Hr.				1000 Hr.				5000 Hr.			
	Rupture		0.5% Creep strain		Rupture		0.5% Creep strain		Rupture		0.5% Creep strain	
	Stress, p.s.i.	Min. creep rate, % per hr.	Stress, p.s.i.	Min. creep rate, % per hr.	Stress, p.s.i.	Min. creep rate, % per hr.	Stress, p.s.i.	Min. creep rate, % per hr.	Stress, p.s.i.	Min. creep rate, % per hr.	Stress, p.s.i.	Min. creep rate, % per hr.
73J(3)	35,000	0.035	Not available		28,000	0.0083	Not available		24,000	0.0031	Not available	
95M255	40,000	0.033	29,500	0.0017	27,000	0.0022	21,000	0.0012	21,000	0.0011	16,500	0.0007
90M158	36,000	0.0025	32,000	0.0022	26,000	0.0016	21,000	0.0014	20,000	0.0008	16,000	0.0006

TABLE XIII

CREEP-RUPTURE DATA AT 815° C. (1500° F.), SUMMARIZED ON A MINIMUM CREEP RATE BASIS

Minimum creep rate, % per hr.	Alloy 73J(3)		Alloy 95M255		Alloy 90M158	
	Stress, p.s.i.	Hours to rupture	Stress, p.s.i.	Hours to rupture	Stress, p.s.i.	Hours to rupture
0.05	37,000	56	42,000	70		
0.01	29,500	570	35,000	300		
0.005	26,000	2,000	32,000	400		
0.002	22,000	10,000	26,000	1,200	32,000	200
0.001	20,000		20,000	5,000	22,000	3,000

Metallography of Creep-Rupture Test Bars

The microstructures of the test bars produced from the alloys listed in Table IX are presented in Figs. 26 to 39.

To reveal the complete microstructure of Alloy 53M104, as shown in Figs. 26 and 27, a double etching technique was employed. An alcohol solution of ferric chloride and hydrochloric acid was used to bring out the light gray areas but this reagent alone would not clearly reveal the eutectic network. In order to bring out this eutectic network an electrolytic etch was employed, using an aqueous solution of sodium cyanide as the electrolyte. With this etch it was necessary to use care to avoid over-etching. About 5 to 15 secs. at 1 to 3 v. was adequate. Neither the electrolytic etch nor the acid etch alone revealed the complete microstructure.

Alloys 90M158 and 95M255 etched satisfactorily with the electrolytic technique alone (see Figs. 28 to 31 and 34 to 37). However, as a further aid in studying the phases present in these alloys and also in studying structural changes that took place during creep-rupture testing, Figs. 32 and 33 are included. These show the microstructure of Alloy 90M158 at 1500 diameters as revealed by a modified chrome-regia etch.

It was found difficult to reveal the microstructure of Alloy 258M252 in a satisfactory manner. The reagent selected, nitric acid plus acetic acid in acetone, seemed to be the most effective.

Discussion of Metallography as Related to Creep-Rupture Properties

At this stage it is not possible positively to identify all phases revealed in the microstructure of the alloys studied.

The electrolytic etch has shown that a phase that occurs in a eutectic manner is common to Alloys 53M104, 90M158, and 95M255. This phase is attacked and darkened by this electrolytic etching. Figs. 26 to 31 and 34 to 37 will illustrate this point. The identity of this phase has previously been tentatively established as NiMo.

It will be noted that the matrix of Alloy 53M104 (see Figs. 26 and 27) consists of a gray etching phase and a clear white phase. This gray phase is etched by the ferric chloride – hydrochloric acid etch and has been tentatively identified as NiAl. It is significant that this alloy, 53M104, which is the only alloy tested that contains this NiAl phase, yielded the poorest creep-rupture properties. A similar etching technique applied to Alloys 90M158, 95M255, and 258M252 failed to reveal a similar phase.

The two alloys that gave the best creep-rupture performance at 1500° F. possessed similar microstructures, as may be seen from Figs. 28 to 31 and 34 to 37. This microstructure consists of:

(*a*) The previously mentioned NiMo eutectic phase that is darkened by the electrolytic etch.

(*b*) Clear white areas usually associated with NiMo eutectic. By reference to Fig. 10, these areas are tentatively identified as Ni_3Al and were originally the alpha-Ni_3Al eutectic (1).

(*c*) A mottled background that at a high magnification (see Figs. 29, 32, and 35) is seen to be a dark-etching, very fine network in a white background. The network is tentatively identified as Ni_3Al and the background as alpha (see Figs 10 and 11).

The clear white areas of Ni_3Al are more numerous in Alloy 90M158 and the NiMo eutectic is more prevalent and continuous in Alloy 95M255 (see Figs. 28 and 34). It is considered significant that these two microstructural features are always associated with each other; this helps to confirm the possibility that the clear Ni_3Al areas are eutectic in origin.

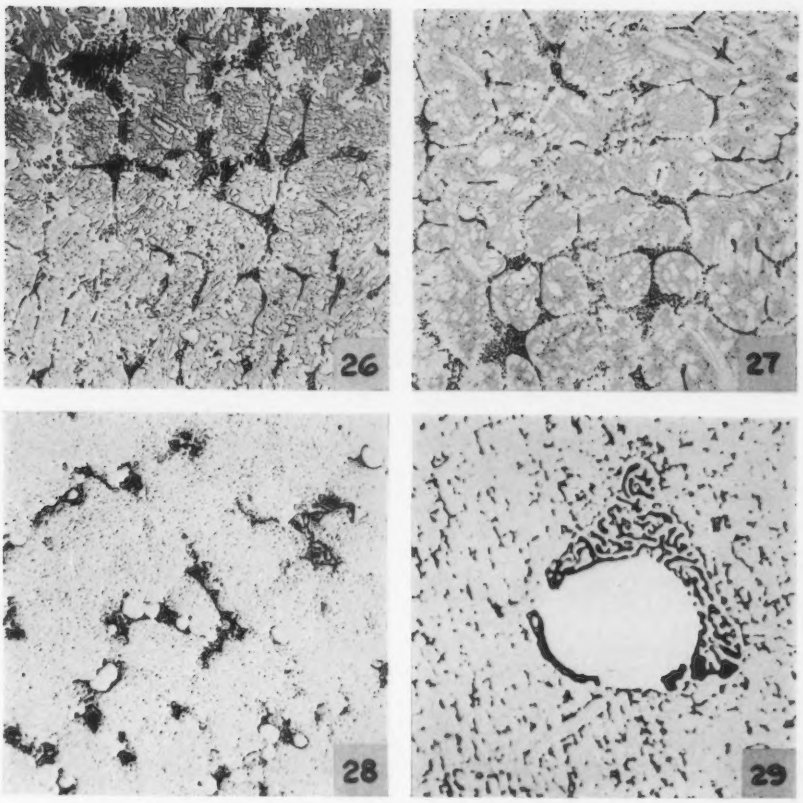

FIG. 26. *Alloy 53M104, as cast. Etched five seconds in ferric chloride plus hydrochloric acid in alcohol, and 15 sec. electrolytically in 10% sodium cyanide at 3 v. ×200. Ni, 74.9%; Al, 14.2%; Mo, 10.4%.*

FIG. 27. *Alloy 53M104, after creep-rupture test at 1500° F. for 27 hr. Etched five seconds in ferric chloride plus hydrochloric acid in alcohol, and 15 sec. electrolytically in 10% sodium cyanide at 3 v. ×200. Ni, 74.9%; Al, 14.2%; Mo, 10.4%.*

FIG. 28. *Alloy 90M158, as cast. Electrolytic etch: 10% sodium cyanide at 3 v. ×200. Ni, 75.6%; Al, 8.4%; Mo, 15.8%.*

FIG. 29. *Same as Fig. 28. ×1500.*

PLATE V

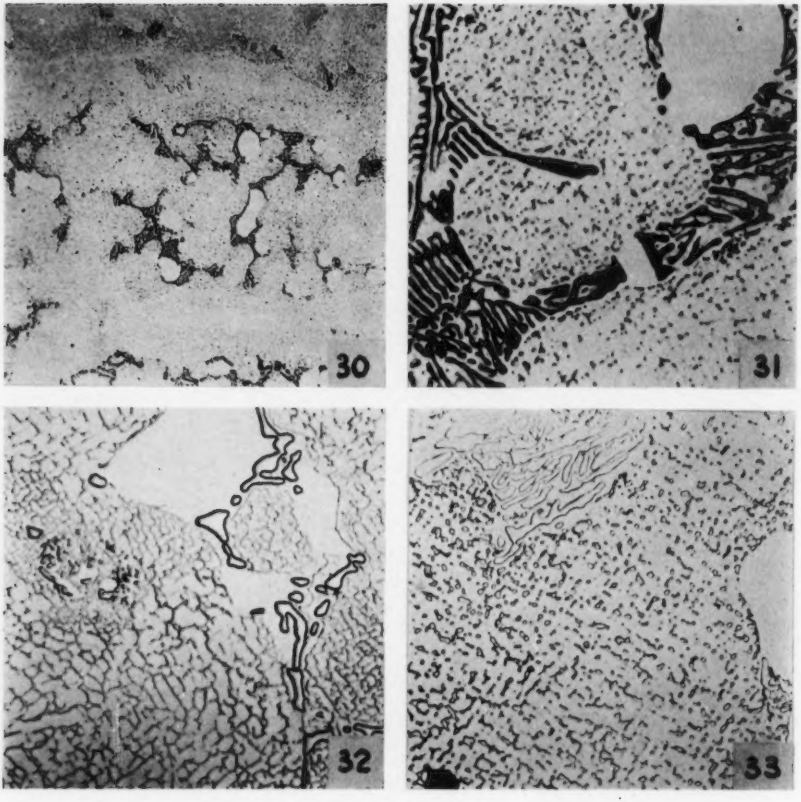

FIG. 30. *Alloy 90M158, after creep-rupture testing at 815° C. (1500° F.) for 680 hr. Electrolytic etch in 10% sodium cyanide at 3 v.* ×*200.*

FIG. 31. *Same as Fig. 30.* ×*1500.*

FIG. 32. *Alloy 90M158, as cast. Etchant: alcoholic chrome regia.* ×*1500.*

FIG. 33. *Alloy 90M158, after 680 hr. creep-rupture testing at 815° C. (1500° F.). Etchant: alcoholic chrome regia.* ×*1500.*

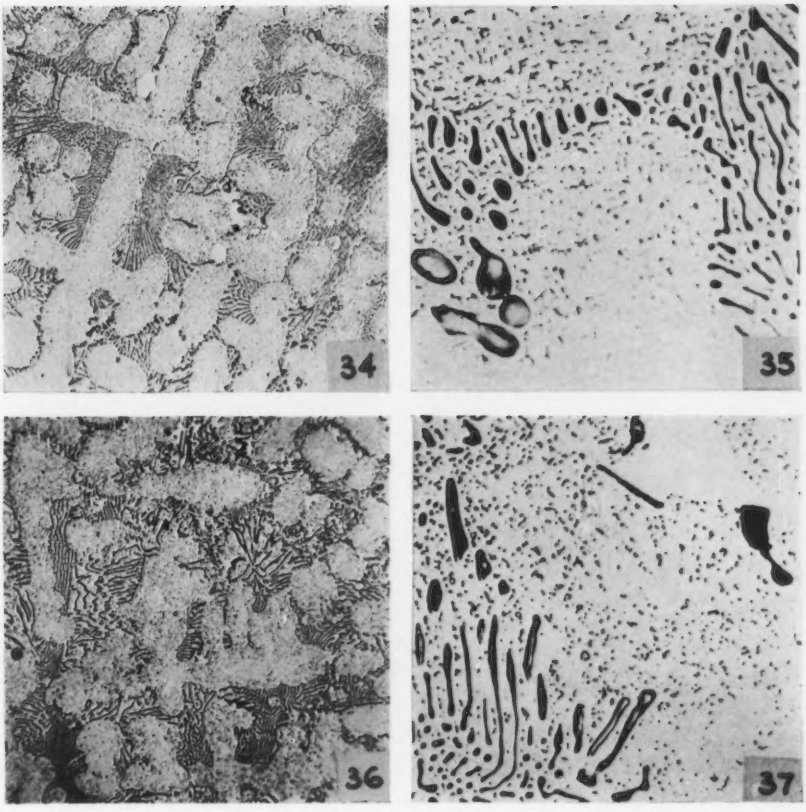

FIG. 34. *Alloy 95M255, as cast. Electrolytic etch: 10% sodium cyanide at 3 v.* ×*200. Ni, 66.5%; Al, 7.0%; Mo, 25.5%.*

FIG. 35. *Same as Fig. 34.* ×*1500.*

FIG. 36. *Alloy 95M255, after creep-rupture testing at 815° C. (1500° F.) for 930 hr. Electrolytic etch: 10% sodium cyanide at 3 v.* ×*200.*

FIG. 37. *Same as Fig. 36.* ×*1500.*

PLATE VII

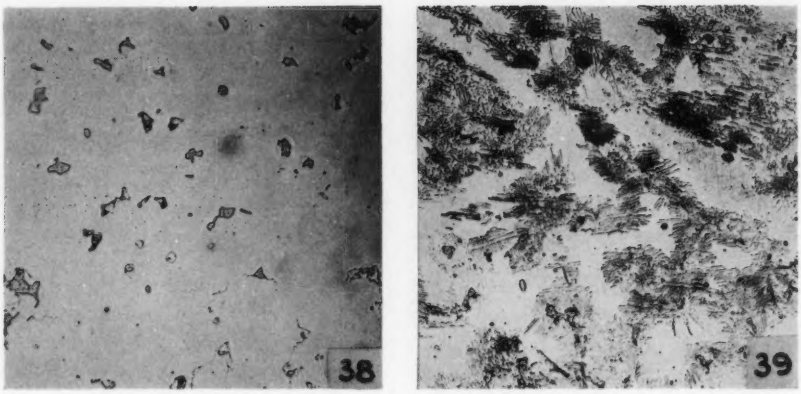

FIG. 38. *Alloy 258M252, as cast. Etch: nitric acid plus acetic acid in acetone. ×200. Ni, 72.4%; Al, 2.8%; Mo, 25.2%.*

FIG. 39. *Alloy 258M252, after creep-rupture testing at 815° C. (1500° F.) for 460 hr. Etch: nitric acid plus acetic acid in acetone. ×200. Ni, 72.4%; Al, 2.8%; Mo, 25.2%.*

After exposure to the temperature of testing at 815° C. (1500° F.) there is evidence that the Ni_3Al network has coalesced. A comparison of Fig. 29 with Fig. 31, and of Fig. 35 with Fig. 37, will illustrate this.

Further to study the phases present in Alloys 90M158 and 95M255, various other etching reagents were employed. A modified alcoholic solution of chrome-regia seemed to be the most useful. The microstructures of Alloy 90M158 (as developed by this reagent), both before and after creep-rupture testing, are shown at a magnification of ×1500 in Figs. 32 and 33. The NiMo eutectic phase that was darkened by the electrolytic etch was only outlined by the chrome-regia etch. The network structure shown in Fig. 29 has been brought out more clearly by this chrome-regia etch in Fig. 32. The effect on this network of prolonged exposure to a temperature of 815° C. (1500° F.) is well illustrated by Fig. 31. Here the coalescence of this network phase is unmistakable.

The fourth alloy tested, 248M252, is not of much interest since its properties were quite inferior. Its microstructure, as shown in Fig. 38, is largely single-phase, probably alpha solid solution, with small patches of a second phase which can be resolved into a eutectic-like appearance at high magnification. The microstructure is radically altered during creep-rupture testing, as may be seen in Fig. 39. From a study of Ellinger's work (2), this new phase in Fig. 39 would appear to be the nickel–molybdenum phase, gamma (Ni_3Mo).

General Conclusions

It is evident that the work reported in this paper has provided the starting point for the development of an entirely new series of high temperature alloys based on nickel, aluminum, and one or more other elements, such as molybdenum.

There is evidence that the microstructure of these alloys may be used as a criterion of their usefulness, since any alloy containing an appreciable proportion of the phase NiAl would not be expected to be suitable.

While most of the data presented are only the results of single melts and single tests, the indications are nevertheless quite promising. One of the alloys produced (95M255) compares quite favorably with the best of other known high temperature alloys. Alloys of this new series are readily melted by high frequency induction and present no unusual casting difficulties.

Acknowledgments

This work has been made possible through the co-operation of the Bureau of Mines and the National Research Council's Associate Committee on High Temperature Metals. Grateful acknowledgment is made for assistance and advice received, during the preparation of this paper, from H. H. Bleakney,

Associate Research Officer of the National Research Council and secretary of the Associate Committee on High Temperature Metals. It is also desired to acknowledge the work of R. F. Cole, presently of the Ford Motor Company of Canada, Limited, who assisted in the earlier stages of this project.

References

1. ALEXANDER, W. O. and VAUGHAN, N. B. J. Inst. Metals, 61 : 247-260. 1937.
2. ELLINGER, F. H. Trans. Am. Soc. Metals, 30 : 607-638. 1942.
3. EPREMIAN, E. Trans. Am. Soc. Metals, 39 : 261-280. 1947.
4. GRANT, N. J. Trans. Am. Soc. Metals, 40 : 585-616. 1948.